THE UNIVERSITY OF OKLAHOMA

GRADUATE COLLEGE

EXCITATION OF ARGON ATOMS BY ELECTRON IMPACT

A DISSERTATION

SUBMITTED TO THE GRADUATE FACULTY

in partial fulfillment of the requirements

for the degree of

DOCTOR OF PHILOSOPHY

BY

JAMES KNOXFORD BALLOU, JR.

Norman, Oklahoma

1973

EXCITATION OF ARGON ATOMS BY ELECTRON IMPACT

APPROVED BY

C C Lin

Robert M St. John

S. E. Babb Jr.

W. J. Fitzpatrick

William N. Huff

DISSERTATION COMMITTEE

ABSTRACT

Electron excitation functions of some thirty states of the $3p^5ns$, $3p^5np$, and $3p^5nd$ configurations of the argon atom have been measured by the optical method. In order to evaluate the level cross sections from the optical excitation cross sections we have experimentally determined the branching ratios by measuring the flux ratios for lines originating on the levels of interest. Since the electron-excited source does not provide sufficient intensity to measure the flux ratios, and since the flux ratios do not depend on the manner in which the level of interest is populated a much more intense radio frequency (100 MHz) argon discharge was used as a source for the flux ratio measurements. This procedure gives more accurate level cross sections than does the conventional approach of using theoretical transition probabilities to form the branching ratios since for an atom as complex as argon the wave functions of the excited states calculated by a semiempirical treatment of the fine structure are not always of sufficient accuracy to give reliable transition probabilities. Analysis of the shape of the excitation functions is facilitated by expressing the wave functions of the excited states of argon in terms of the LS-eigenfunctions, and the special

features of the experimental data of excitation functions can be readily explained by generalizing the results of helium. Analogous to the case of neon, one can show theoretically that within a configuration $3p^5n\ell$, the states with odd values of $J+\ell$ in general have larger excitation cross sections than the ones with even values at incident energies well above the threshold and that in general $Q(J=0) > Q(J=2)$, $Q(J=1) > Q(J=3)$ for the np states, and $Q(J=1) > Q(J=3)$, $Q(J=2) > Q(J=0,4)$ for nd. The experimental results of the excitation cross sections are found to be in good agreement with these rules.

ACKNOWLEDGEMENTS

I want to thank Professor Chun C. Lin for his guidance and patience during my graduate career.

Also I want to thank all of the people who have contributed to the success of this work; particularly John Thompson and Mike Murray. I also want to especially thank Tony Solomon and John Keto for many stimulating conversations.

I have also received unfailing faith, support, and encouragement from my wife and parents; there is no way I can fully express how much this has meant to me. However, in order to partially express my appreciation, I dedicate this thesis to them.

TABLE OF CONTENTS

		Page
Abstract		iii
Acknowledgements		v
List of Tables		vii
List of Figures		ix
Chapter		
I.	Introduction	1
	More Rigorous Treatment of the Experimental Method	5
II.	Apparatus and Methods	10
	Excitation Function Measurement Procedure	10
	Apparatus for Excitation Function Measurement	14
	Measurement of Absolute Photon Fluxes	21
	Flux Ratio Measurements	26
III.	Structure of Argon	31
IV.	Theory	38
V.	Results	44
	Comparison with other Investigators	44
	2p and 3p Families	45
	4d Family	64
	3s Family	76
	nd'_4	76
VI.	Summary	81

LIST OF TABLES

Table		Page
1.	Examples of the number of states in each configuration, the Paschen notation for this state, and its J.	33
2.	Examples of transitions among groups and their respective wavelength ranges	37
3.	Optical cross sections (at maximum and at 100 eV) measured in units of 10^{-19} cm^2.	49
4.	Optical cross sections for the $2p \rightarrow 1s$ lines at 100 eV in units of 10^{-19} cm^2.	50
5.	Experimental values of the apparent and level cross sections of the 2p states at 100 and 200 eV and comparison with theoretical level cross sections in units of $10^{-19} cm^2$.	51
6.	Flux ratios measured in this experiment for the $3p^5 4p \rightarrow 3p^5 4s$ transitions, and transition probability ratios from Ref. 12.	52
7.	Flux ratios measured in this experiment for the $3p^5 5p \rightarrow 3p^5 4s$ transitions, and transition probability ratios from Ref. 12.	57
8.	Comparison of the transition probabilities for the $3p \rightarrow 1s$ group and the transition probabilities of the $3p \rightarrow 3d$ transitions reported by Wiese *et al*[13].	60
9.	Optical cross sections (at maximum and at 100 eV) measured in units of $10^{-19} cm^2$.	61
10.	Optical cross sections at 100 eV for the $3p \rightarrow 1s$ lines in units of $10^{-19} cm^2$.	62
11.	Experimental values of the apparent excitation cross sections and the theoretical level cross sections (by Born approximation) at 100 and 200 eV in units of $10^{-19} cm^2$.	63

Table Page

12. Optical cross sections (at maximum and at 100 eV) for 4d→2p lines measured in units of 10^{-19} cm^2. 66

13. Optical cross sections of the 4d→2p lines at 100 eV in units of 10^{-19} cm^2. 67

14. Flux ratios measured in this experiment for the $3p^5 4d \rightarrow 3p^5 4p$ transitions, and transition probability ratios from Ref. 12. 70

15. Experimental values of the apparent excitation cross sections of the 4d states at 100 and 200 eV and the theoretical level cross sections in units of 10^{-19} cm^2. 73

LIST OF FIGURES

Figure		Page
1.	Illustration of how a particular state f is populated.	2
2.	Configuration of system used to measure excitation functions.	11
3.	Configuration of system used to calibrate optical system.	12
4.	Detail of electron gun grid configuration.	17
5.	Schematic of constant current control.	19
6.	Simplified optical diagram.	24
7.	Optical configuration for the infrared flux ratio experiment.	30
8.	Relative positions of states of several configurations.	35
9.	Excitation functions for 2p→1s lines.	46
10.	Excitation functions for 3p→1s lines.	56
11.	Excitation functions for 4d→2p lines.	65
12.	Excitation functions for 3s→2p lines.	77
13.	Excitation functions for $5d'_4$ and $6d'_4$.	79
14.	Excitation functions for $9d'_4$ and $7d'_4$.	80

CHAPTER I

INTRODUCTION

In this work we wish to study the inelastic collisions of ground-state argon atoms and electrons, by first of all measuring the rates of population of some of the excited states of argon and then correlating these rates of population with the atomic structure and composition of the argon wavefunctions.

The concept of the experiment is to pass a monoenergetic beam of electrons through a container of gas and to utilize the radiation from the excited atoms to determine the rate of population of the excited states. Of course, there are processes other than excitation going on at the same time; however, these processes can usually be made to have a negligible effect on the excitation process. Figure 1 is a schematic of the step-by-step process used to obtain the population of a specific state f. Some of the ground-state (g) atoms within the volume of the electron beam suffer collisions with electrons and are excited to various upper levels, including the state f. In a short time a steady state condition is reached in which the rate of population of f is equal to the rate of depopulation of f. Since the rate of population is made up of two components (the direct

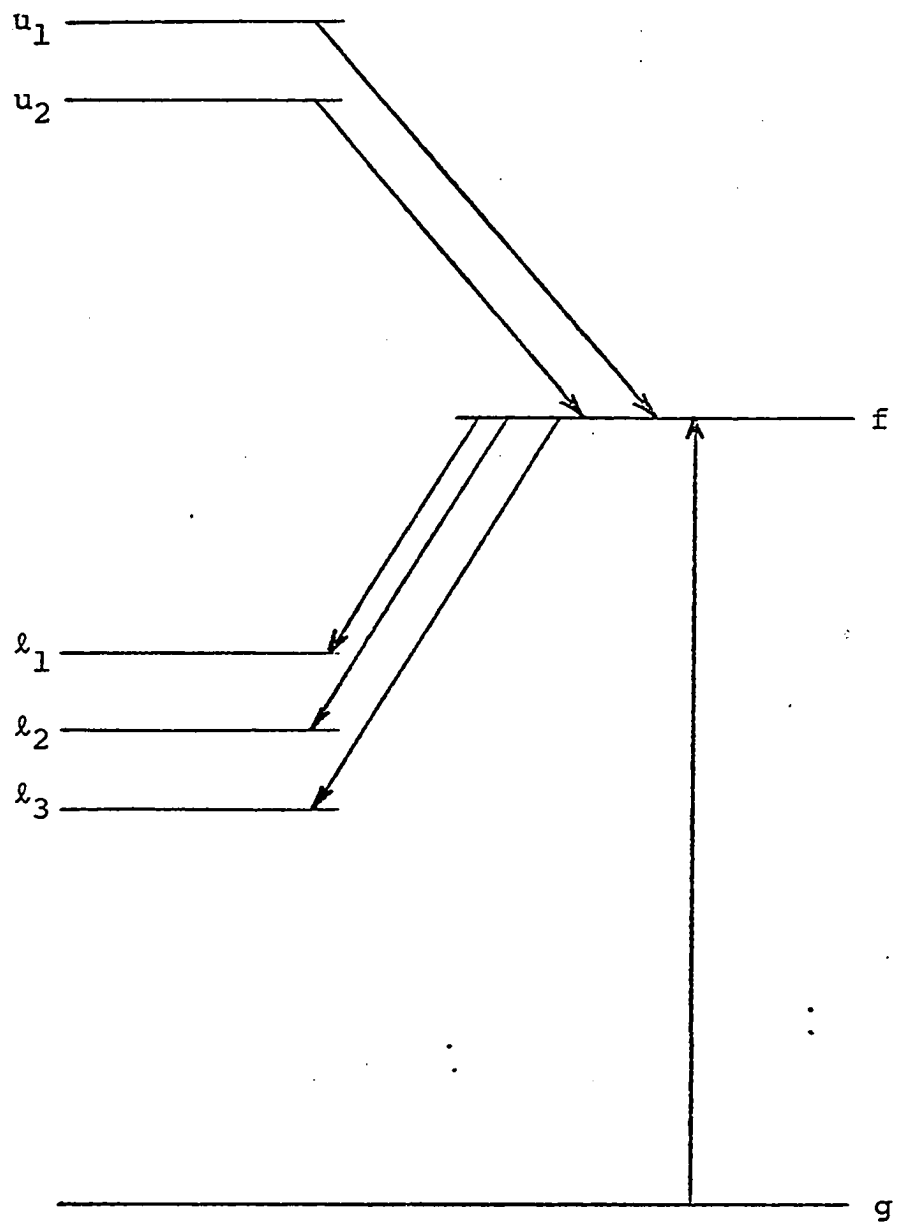

Figure 1. Illustration of how a particular state f is populated.

excitation part and the part due to cascade from upper levels), we find it necessary to determine the rate of depopulation as well as the rate due to cascade, so that by subtracting these rates, we get the rate due to direct excitation.

Ideally the rate of depopulation can be obtained by measuring the absolute photon flux of each line beginning on f and ending on a lower state ℓ (Figure 1), and then form the sum of these fluxes, which yields the rate of depopulation. However, it rarely happens that one can measure the fluxes of all of these lines, since some of them may be in an unfavorable spectral region or may have neighbor lines that can not be separated from a line of interest with an acceptable signal to noise ratio. The photon fluxes of lines that can not be observed in the electron excited source cannot be neglected since the sum of all of these lines may introduce a sizable error. So an alternative procedure is normally used based on the fact that the ratio of the photon fluxes of lines starting on the same upper level is equal to the ratio of their transition probabilities

$$\frac{I_1}{I_2} = \frac{A_{f1}}{A_{f2}} \qquad (1)$$

where I_1, I_2 are the photon fluxes of the lines $f \to \ell_1$ and $f \to \ell_2$ and A_{f1}, A_{f2} are the transition probabilities of the same lines. For some atoms like He and Na, theory gives very good transition probabilities and these are normally used to infer the missing photon fluxes and thus obtain the rate of

depopulation. Theorical transition probabilities in argon, however, are not dependable enough to use in this way so a different scheme was developed. Since the ratio of photon fluxes of lines with a common upper level is independent of how the atom was excited, one may use an argon light source much brighter than the electron excited one to obtain the necessary ratios from

$$\left(\frac{I_1}{I_2}\right)_b = \left(\frac{I_1}{I_2}\right)_{r\text{-}f} \qquad (2)$$

where b indicates that the electron excited source was used and r-f indicates that a r-f (radio frequency) discharge was used.

In summary, the method used to obtain the rate of depopulation of a given state is to measure as many absolute photon fluxes of lines that originate on the state as possible using the electron beam excited source and infer the intensities of the missing lines using experimentally determined intensity ratios from a much brighter source.

The next step is to investigate the ways that f is populated. Under appropriate experimental conditions, it is populated by direct excitation and by cascade from higher levels. If the cascade contribution is subtracted from the rate of depopulation just obtained, then the rate of population of f by electron impact is determined.

The ideal way to account for the cascade contribution is to measure the absolute intensity of each line that adds to the population of f. Take the sum of these intensities

and deduct it from the rate of depopulation. This is not a practical procedure because so many lines can not be measured that an incomplete picture can result. The technique just described, using an intense source to get the necessary ratios to infer the missing photon fluxes, can be used and thus a more reasonable estimate of the rate of population by cascade can be obtained. Once this rate of population is determined the direct cross section can be obtained.

We are also interested in the variation of the population as we vary the incident electron energy. This is called the excitation function, and it is measured by observing the flux variation of a line as the electron energy is varied.

More Rigorous Treatment of the Experimental Method

In this section we will take a much closer look at the optical method and derive the first set of relations used to obtain the cross sections from the experimental measurements. The point of view will be slightly different from the last section. Here we will first derive the relation between the absolute photon flux of one line to the direct excitation cross section of the level and then generalize the method to include the photon flux of more than one line from the same upper level.

The time rate of change of the population density of f can be written as

$$\frac{dn_f}{dt} = NnvQ(f) - \sum_{\ell<f} A_{f\ell} n_f + \sum_{u>f} A_{uf} n_u \qquad (3)$$

where n_f is the number density of excited atoms in state f, N is the number density of ground state atoms, n (without subscript) is the number density of projectile electrons in the beam, v is the electron velocity, Q(f) is the direct excitation cross section of state f in units of area, the summation over the indices u and ℓ represent summations over all levels with greater energy than f and summation over levels with less energy than f respectively, A_{uf} is the spontaneous transition probability from some upper state u to f, $A_{f\ell}$ is the spontaneous transition probability from state f to some lower state ℓ, and n_u is the number density of atoms in some upper state u. The first term on the right is the rate of excitation of f from the ground state, the second term is the rate of depopulation via radiation, and the third term is the rate of population cascade from higher levels. For steady state conditions

$$\frac{dn_f}{dt} = 0 \qquad (4)$$

and solving equation (3) for n_f using equation (4) yields the steady state population density of f

$$n_f = \frac{1}{\sum_{\ell} A_f} \left[NnvQ(f) + \sum_{u} A_{uf} n_u \right] . \qquad (5)$$

The photon flux emitted in the f to ℓ transition is

$$J_{f\ell} = n_f A_{f\ell} S \qquad (6)$$

where $J_{f\ell}$ is the photon flux in number of photons per second

per unit length of electron path and S is the cross sectional area of the beam. The definition of current density j is

$$j=nve \tag{7}$$

where e is the electronic charge, and the relation between total current and j is

$$I = jS = nveS. \tag{8}$$

Now one may use equations (6), (7) along with (8) to obtain an expression for Q(f)

$$Q(f) = \frac{\sum_{\ell'} A_{f\ell'}}{A_{f\ell}} \frac{e}{NI} J_{f\ell} - \sum_{u} \frac{e}{NI} J_{uf}. \tag{9}$$

In equation (9) notice that the photon fluxes are all multiplied by $\frac{e}{NI}$, and that each of the two terms $\frac{e}{NI}$ times the absolute photon fluxes, has dimensions of area, and that each of them has been "normalized" with respect to N and I so that one may compare them even if measured under slightly different conditions. For these reasons it is convenient to define

$$Q_{f\ell} = \frac{e}{NI} J_{f\ell} \tag{10}$$

where $Q_{f\ell}$ is called the optical cross section of the f to ℓ transition. Rewriting equation (9) in view of (10)

$$Q(f) = \frac{\sum_{\ell'} A_{f\ell'}}{A_{f\ell}} Q_{f\ell} - \sum_{u} Q_{uf}. \tag{11}$$

The factor $\frac{\sum_{\ell'} A_{f\ell'}}{A_{f\ell}}$ in the first term on the right of equation (11) is just the factor needed to account for the fact that f is depopulated via several transitions to lower levels. This factor is the branching ratio. So now the first term can be seen to represent the rate of population. In terms of the previous section this term is the sum of the optical cross sections of all lines that have f as their upper level. So, as mentioned in the preceding section, the most consistant way to evaluate the first term is to measure the optical cross section of each of these lines and then form the sum. This is often impossible for the reasons stated earlier, so the branching ratios are often formed from theoretical transition probabilities. For some atoms, like He and Na, theory yields excellent transition probabilities; however for argon the theoretical transition probabilities sometimes are not very reliable and so we hesitate to use them. This is why we developed the following scheme to account for the optical cross sections of these missing lines.

Basically, the scheme is to use the fact that the ratios of absolute photon fluxes of lines that have a common upper level are independent of how the upper state is populated, and since the missing optical cross sections are missing because of a lack of intensity, a much brighter argon source is used. For example if Q_{f1} is missing from the electron-beam data and Q_{f2} is not, then

$$Q_{f1} = Q_{f2} \frac{I_{f1}}{I_{f2}} \qquad (12)$$

where I_{f1} is the photon flux of the $f \rightarrow \ell_1$ transition, and I_{f2} is the photon flux from the $f \rightarrow \ell_2$ transition both measured from the brighter argon source.

In this section we have developed the relation between the absolute photon flux of a line and the rate of population of a level; defined cross sections that essentially normalizes the population rates; shown how the optical cross sections of many lines relate to the level cross section; shown how the cross sections of missing lines can be inferred from flux ratio data and accounted for in a systematic way. The next chapter will discuss the apparatus and measurement methods used.

CHAPTER II

APPARATUS AND METHODS

The apparatus may be divided into four parts: the vacuum system, the electron gun, the electronics, and the optics. Figure 2 is a simplified sketch of the apparatus as it is used to measure excitation functions. Figure 3 is a schematic of the apparatus configuration used to calibrate the optics for the absolute light intensity measurements. Sections I and II of this chapter will describe the excitation function measurement procedure and apparatus. The absolute photon flux calibration and measurement procedures are discussed, as well as the flux ratio methods, in Sections III and IV.

Section I - Excitation Function Measurement Procedure

An optical excitation function is the variation of the light intensity of a spectral line as the energy of the exciting electrons is varied in a monotonic fashion. This section describes how this measurement is made and a schematic of the apparatus is discussed.

Figure 2 illustrates the overall function of the system and its parts. The experiment is carried out in the collision chamber of the vacuum system, which is equipped

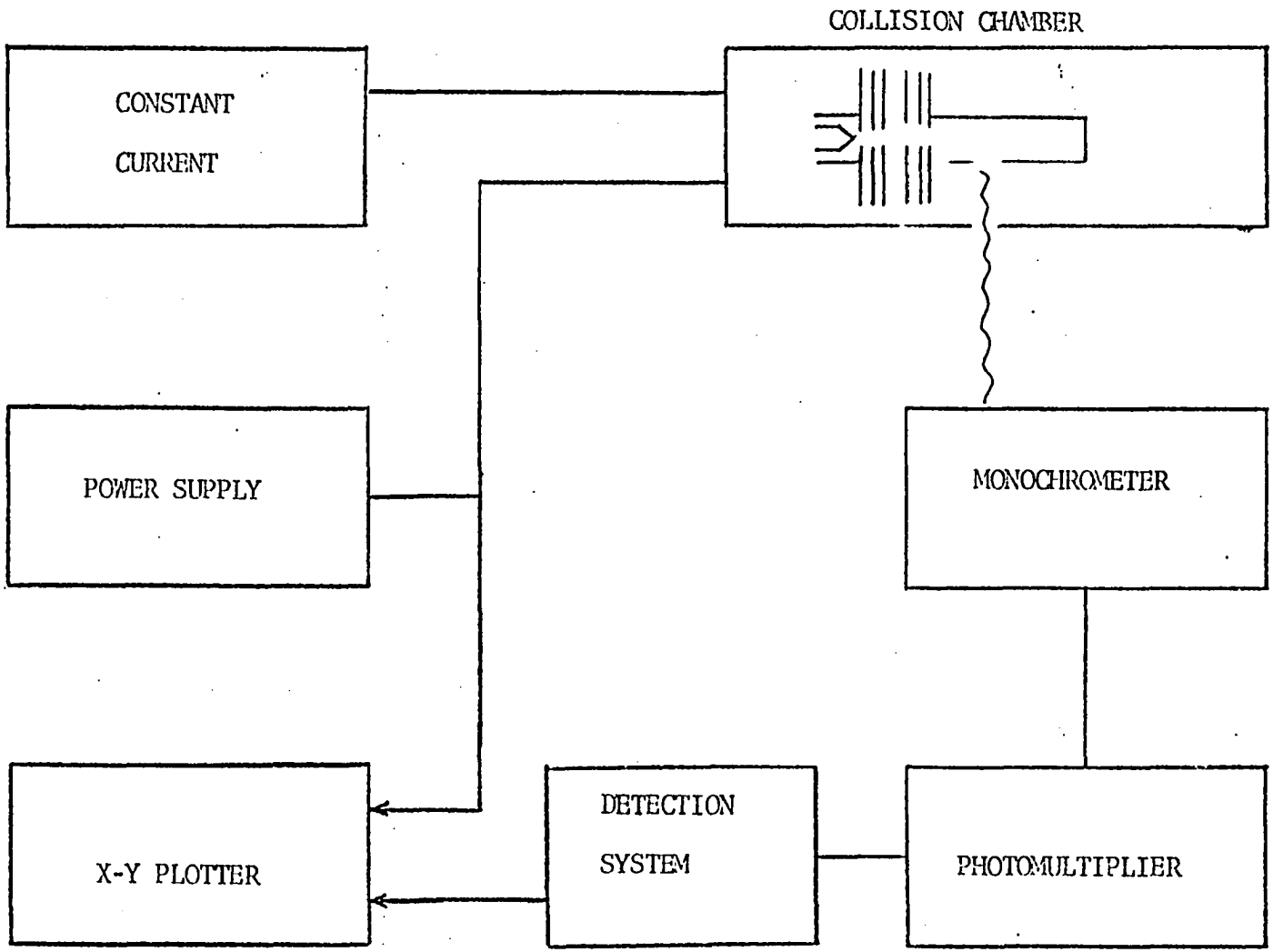

Figure 2. Configuration of system used to measure excition functions.

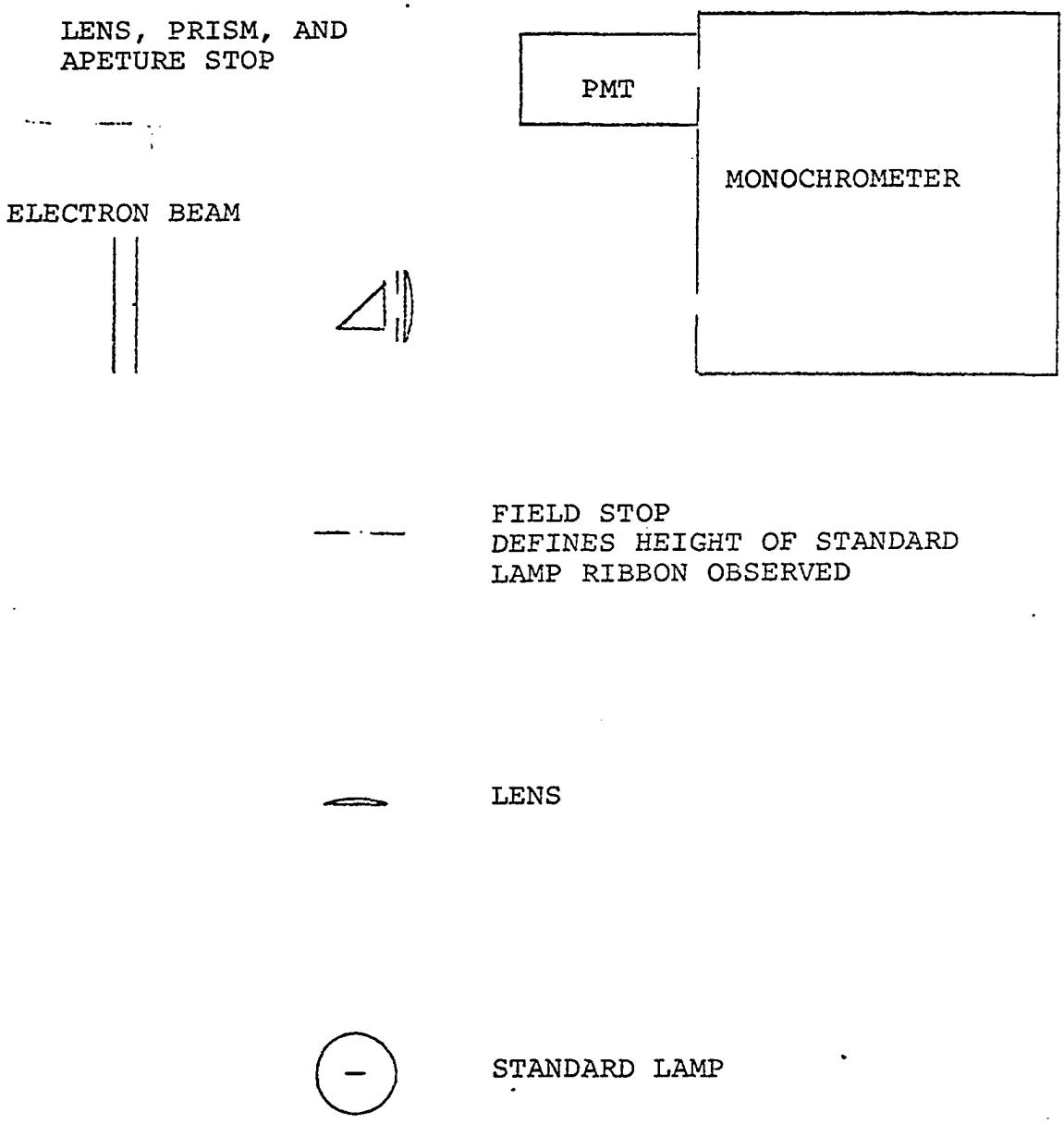

Figure 3. Configuration of system used to calibrate optical system. The prism is removed to observe the electron beam.

with an electron gun that produces a monoenergetic beam of electrons and directs them into a shielded faraday cup which serves as an electrostatic shield, electron collector, and observation region. The light produced by the excited atoms in the argon filled collision chamber is focused onto a slit of a monochrometer which separates the spectrum and allows only a narrow region of the spectrum through the exit slit onto the cathode of a photomultiplier. The output of the photomultiplier is processed by a linear detection system and fed into the Y-axis input of an X-Y plotter.

Since the object of this part of the experiment is to obtain a plot of the photon flux verses incident electron energy, the energy is varied by a swept power supply whose output is also used to drive the X-axis of the X-Y plotter. Thus we obtain a plot of the photon flux (Y-axis) verses the electron energy (X-axis).

One other problem remains, and that is the electron current varies as the electron energy is changed, and since the line intensity is directly proportional to the beam current one must either divide the signal for each energy by the current or one must hold the current constant during the run. We have chosen the latter method. In brief, a constant current device was constructed which senses the current and detects any variance from a reference current and then applies a correction voltage to the control grid of the electron gun thus holding the beam current constant.

A more detailed discussion of each of these pieces of apparatus follows in the next section.

Section II - Apparatus for Excitation Function Measurement

Vacuum System

The vacuum system consists of the experimental region, pumps, gas handling system, and pressure measuring devices. The experimental region is constructed of 3" I.D. pyrex pipeline tee with 1" I.D. side ports, and joined to the other sections of the vacuum system with 1" I.D. pyrex pipeline through a stainless steel valve and a glass to metal seal. One of the ports of the 3" I.D. tee is used to mount a quartz window to allow radiation to escape, and the other is blanked off and not used. The rest of the system is blown glass of standard construction.

The experimental chamber is equipped with a Bendix sorption pump to remove gases evolved from hot electron gun parts and thus help insure sample purity.

The rest of the pumping system consists of a 2" I.D. CVC diffusion pump backed up with a Welch Duo Seal forepump. An orbitron ion pump is also used to help maintain the system.

The gas samples were Linde research grade supplied in one liter pyrex flasks. Each sample was connected to a manifold via a double stopcock system that allowed small doses to be introduced into the system. Three types of

samples were maintained on the system; argon, neon, and helium. Neon and helium were used to test system performance.

During the experiment a measure of the sample pressure was obtained by using a McLeod gauge. The collision region was isolated from the possible mercury contamination from the McLeod gauge by two liquid nitrogen cold traps; one near the McLeod gauge and the other the main system cold trap.

During operation, both cold traps were filled, the main pumps valved off, and the sample introduced into the system. The sorption pump was left on during the experiment. With the system in this configuration no foreign gas spectra could be observed, nor could a pressure increase be measured with the McLeod gauge after 10 hours of operation.

Electron Gun

The purpose of the electron gun is to produce a well defined beam of nearly monoenergetic electrons at energies as low as 13 eV and at sufficient beam currents to produce observable line intensities. For most lines, at low energies, about 50 microamps is necessary for good signal to noise ratios. The electron gun normally delivered 100 microamps at these energies.

The design of the electron gun is the pentode type described by Sharpton and Anderson[1,2] with a few modifications. First, the electron source is a tungsten wire hairpin of

5 or 6 thousandths of an inch diameter instead of an indirectly heated dispenser cathode. The dispenser cathode was found to be hard to use and have a short life, while the tungsten hairpin is rugged, has excellent emission properties, and a long life. Second, a grounded shield is provided around the faraday cup to help prevent stray currents from being collected by the faraday cup. Third, the internal structure of the faraday cup is different; in previous guns grounded grids and suppressor cups were provided to suppress the secondary electron current and to insure complete electron collection. But by performing several experiments on electrons scattered by the electron collector, it was determined that the best way to insure complete electron collection was to make the solid angle of escape for electrons that hit the back of the faraday cup very small. In the same view, one source[3] claims that the ratio of the entrance diameter to the length of the faraday cup should be 1:10 for 95% collection efficiency. In this case it is 1:24.

Figure 4 is a diagram of the grid structure of the electron gun. The grids are made of 304 stainless steel with a 125 mil center hole. The grids and most other gun parts are standardized and manufactured by Physicon, Inc.

The cathode, control grid, focus grid, and suppressor are all operated at potentials referenced to the electron energy. This set of grids form an electron extractor, whose purpose is to extract the electrons from the cathode

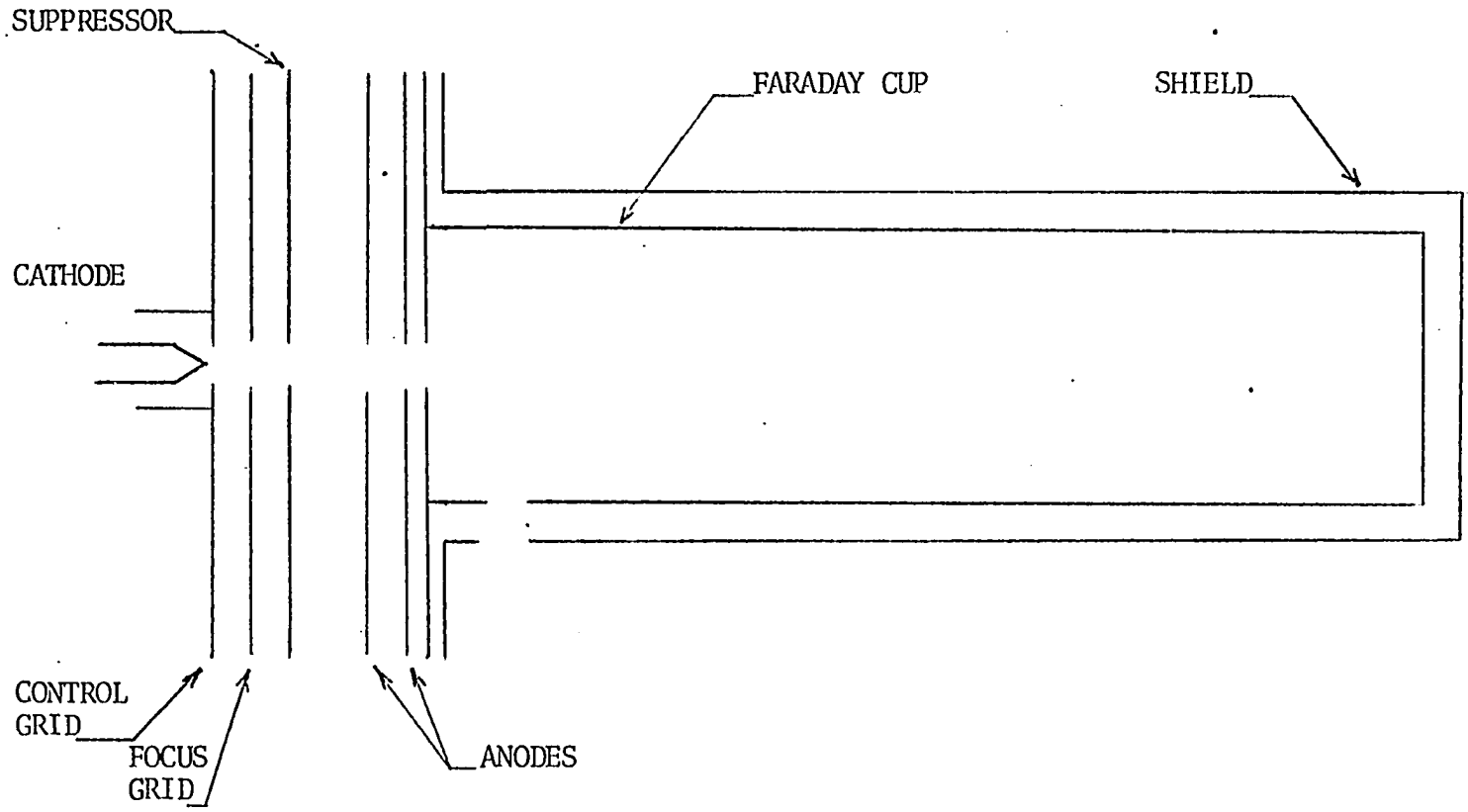

Figure 4. Detail of electron gun grid configuration.

region, provide for electron current control and to form a virtual cathode near the suppressor grid. The control grid is run negative with respect to one leg of the filament cathode; the focus grid is run at about 100 volts positive with respect to the cathode; the suppressor is operated at the cathode potential. The energy of the electrons is determined by the potential between the suppressor and the grounded anodes, which form a drift space, and a buffer region to eliminate field penetration into the faraday cup.

Electronics

The electronics can be separated into two main groups according to function; electronics used to control the electron beam and the detection system used to process the signals from the photomultiplier.

The control electronics consists of the power supplies for the cathode and electron gun grids, the swept power supply for electron energy, and the constant current device. The power supplies for the grids and cathode heater are of conventional design and will not be discussed. The swept power supply is implemented by inserting a ten turn pot into the control chain of a regulated 0-500 volt power supply, when the resistance of the pot is varied by a variable speed-reversible motor the variation of resistance produces the required change in output voltage.

The constant current device is represented in block form in Figure 5. The current collected by the faraday

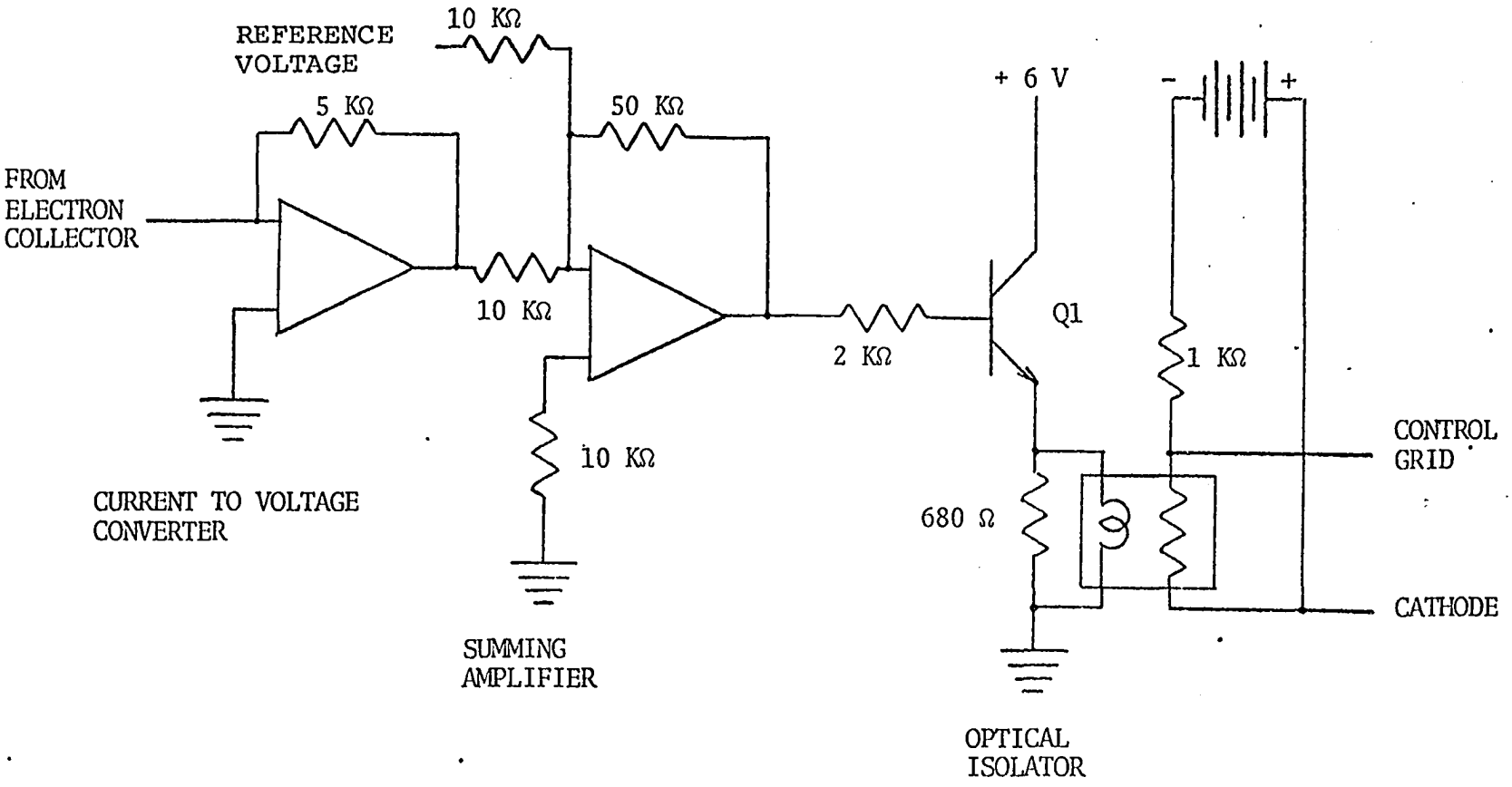

Figure 5. Schematic of Constant Current Control

cup is fed into a current-to-voltage converter and then to a summing amplifier that sums the voltage of the current-to-voltage converter and a reference voltage. If the sum of these voltages is correct, i.e., the electron beam current is at the predetermined level, then a constant bias is applied to the base of transistor Q1. If the beam current should change, the summing amplifier will detect it and apply a different bias to Q1. Q1 than changes the current through an incandescent light that shines on a photoresistor. The photoresistor is part of a voltage divider biased at the cathode potential, that applies the correction voltage to the control grid. The advantage of this system is that it provides a simple way to apply a bias to a grid that is referenced to a point (the cathode) that changes its potential with respect to ground over a large range (∿10-200 volts).

The accuracy of the control has been measured at better than 1 per cent (1 per cent is the lower limit of the test) over the range of 10-200 microamps.

The attractive feature of this control with respect to earlier models[2] is that the current may be changed with only one adjustment--the reference for the summing amplifier.

Several schemes were used over the course of this work to improve the signal to noise ratio of photomultiplier output; wide band amplification and mixing, pulse counting, and phase detection. The system that proved the most useful

and provided all of the data presented here was a Keithly electrometer and an integrating capacitor; the integration time constant was the RC of the capacitor and the large input impedence of the electrometer. The output of the Keithly amplifier provided adequate signal for the X-Y plotter.

Section III - Measurement of Absolute Photon Fluxes

In the measurement of the cross sections for this work the absolute determination of the photon flux of a line is of utmost importance. The definition of the optical cross section of a line is

$$Q_{jk} = \frac{e}{NI} J_{jk} \qquad (13)$$

where e is electron charge, N is the number density of ground state atoms, I is the total electron beam current, and J_{jk} is the number of photons per second per unit length of beam emitted by the excited atoms making the j to k transition. The measurement of J_{jk} is the subject of this section, along with the measurement of the ratios of photon fluxes.

Basic Measurement Method

In this work light is detected by photomultipliers. The output current of photomultipliers is linearly related to the number of photons per second incident upon their cathode, hence in any optical system the signal current

may be written as

$$I = I_\beta + \Phi\Omega\tau(\lambda)E(\lambda) \qquad (14)$$

for a monochromatic source where Φ is the photon flux from the source in number of photons per second per unit solid angle, Ω is the solid angle accepted by optical system, $\tau(\lambda)$ is the transmission of optical system at the wavelength λ, $E(\lambda)$ is the efficiency of the photomultiplier, and I_β is a background current that is easily measured and subtracted. From here on it will be assumed that I_β has been taken care of unless stated otherwise.

Equation (14) adapted for the case of the electron beam source becomes

$$I_c = J_{jk}\frac{\Omega c}{4\pi}\Delta x\tau_c(\lambda)E(\lambda) \qquad (15)$$

where the subscript c indicates the source is the electron beam.

In order to determine J_{jk}, and thus Q_{jk}, we must compare I_c with a standard photon flux. Our known source is a tungsten strip lamp. If we denote the output current produced by this source by I_s, then

$$I_s = A_s\Omega_s \int R(T,\lambda)\tau_s(\lambda)E(\lambda)\, d\lambda \qquad (16)$$

where A_s is the area of the ribbon observed, Ω_s is the solid angle, $R(\lambda)$ is the photon flux of the ribbon at λ, and temperature T, in photons per second per unit area. The integral is included because the ribbon has a continous spectrum rather than a line spectrum and thus the

total radiation received by the photomultiplier is the integral of $R(T,\lambda)\tau(\lambda)E(\lambda)$ over the bandpass of the monochrometer.

If we now assume that $E(\lambda)$ is constant over the monochrometer bandpass, and combine equation (13) and equation (14) and solve for J_{jk} we get

$$J_{jk} = 4\pi \frac{I_c}{I_s} \frac{\Omega_s A_s}{\Omega_c \Delta x} \frac{\int R(T,\lambda)\ \tau_s(\lambda)\ d\lambda}{\tau_c(\lambda)} \qquad (17)$$

Equation (17) has been dealt with at great length by Sharpton[1], who shows that

$$Q_{jk} = 4\pi \frac{I_c}{I_e I_s} \frac{\varepsilon P_{\Delta\lambda}}{N} \frac{\Omega_s A_s}{\Omega_c \Delta x} \qquad (18)$$

where $P_{\Delta\lambda}$ takes care of Planks function, and ε the emissivity of the tungsten, and

$$P_{\Delta\lambda} = \frac{2c\varepsilon\Delta\lambda}{\lambda^4 (\exp[\frac{hc}{\lambda kt}] - 1)} \qquad (19)$$

The geometrical factor $\frac{\Omega_s A_s}{\Omega_c \Delta x}$ can be determined from the elementary properties of thin lenses. With the aid of Figure 6, and when unit magnification is chosen, the elements of this factor can be written as

$$A_{s\ell} = wh, \qquad (20)$$

$$\Delta x = w \qquad (21)$$

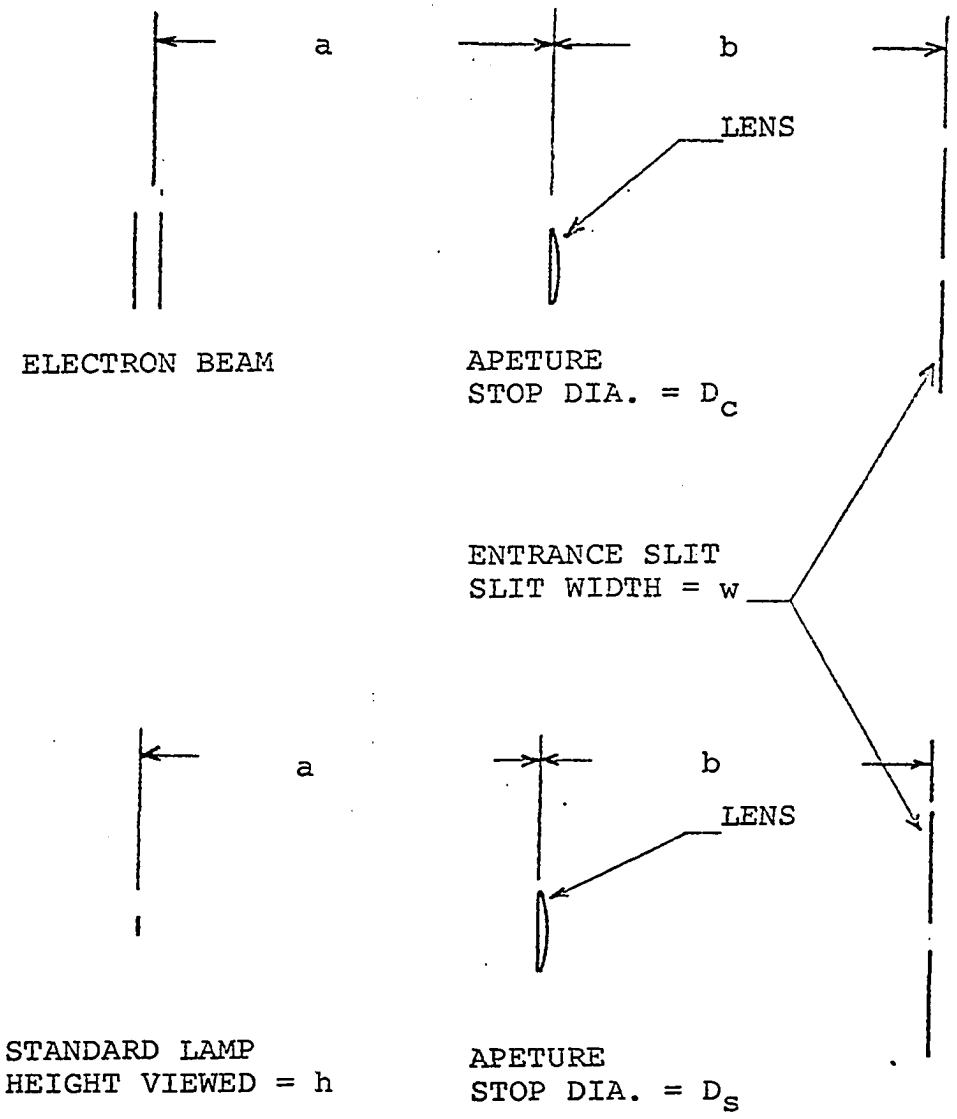

Figure 6. Simplified optical diagram.

$$\Omega_s = \frac{\pi}{4} D_s^2, \tag{22}$$

and

$$\Omega_c = \frac{\pi}{4} D_c^2 \tag{23}$$

where w is the slit width, h is the height of the field stop that determines the height of the standard lamp ribbon used, D_s is the diameter of the apeture stop used to limit the photon flux from the standard lamp, D_c is the diameter of the apeture stop used with the electron-beam source. The factor finally reduces to

$$\frac{\Omega_s A_s}{\Omega_c \Delta x} = h \left(\frac{D_s}{D_c} \right)^2. \tag{24}$$

One has a certain amount of freedom in his choice of h and D_s; h is chosen so that the area of the photocathode illuminated will be about the same size as the area illuminated by the electron-beam source; D_s is chosen so that the standard lamp flux is within about two orders of magnitude of the flux of the electron-beam source. One does not have as much freedom in the choice of D_c, since D_c must be as large as possible to insure that all of the light that can be accepted by the monochrometer will be used. So the effective stop size of the monochrometer must be determined. The technique uses the fact that the throughput of an optical system is directly proportional to the area of its apeture stop, so that

$$\frac{I}{I_1} = \left(\frac{D_c}{D_1}\right)^2 \qquad (25)$$

where I is the photomultiplier current produced by a strong line from the electron-beam when the system is limited by the monochrometer, I_1 is the current produced when a stop of diameter D_1 is used (D_1 must be the limiting stop in this case). We can thus determine D_c from this relation.

Section IV - Flux Ratio Measurements

The factors that effect the flux ratio measurements, and the apparatus used to measure them will be discussed in this section. First of all one must keep in mind that we are not interested in the plasma properties of the r-f discharge, in this experiment, but only in the properties of argon. Common precautions taken to insure that properties of the discharge were not affecting the flux ratios included using only a small segment of the discharge as a source, since the population density of the upper state may vary with position; taking all data relevent to the flux ratios of a particular level in a single run, since there is no guarantee that the population density of a level will be the same from run to run; comparing only the raw data of a run within that run, since the same part of the discharge may not be used from one run to the next. One property of the discharge that was tested repeatly was stability as a function of time and this was found to be excellent; fluxes measured several hours apart

(without turning the discharge off or moving the apparatus) were found to be in excellent agreement.

The r-f discharge itself was a quartz tube 0.8 cm outside diameter and 7.5 cm long. The tube was prepared by evacuating and outgassing the tube and then filling it with argon and operating it for about 24 hours before sealing it off from the vacuum system. The argon pressure in the tube is 1-5 torr; the apparatus used to fill the tube did not allow for a better estimate of the pressure.

The r-f source used most was a standard 100 MHz, 3 watt oscillator. The r-f power was capacitively coupled to the discharge tube. In one set of experiments, the infrared ones, a diathermy machine was used as a power source. In this case, since the diathermy machine operates at about 2 GHz, best results were obtained when the discharge tube was inserted into a running stub and the stub adjusted to give the maximum intensity for a given power level. These infrared flux ratio experiments will be discussed later in this section and again in Chapter V.

The purpose of this section of the experiments is to obtain the absolute photon flux ratios of lines starting on the same upper level; however, it will be shown that using the proper methods one need not actually use the absolute photon fluxes to obtain their ratios if all of the lines from a given level can be detected with a single detector, or if two detectors must be used for two different spectral regions then there must be at least one line common to both detectors.

The number of photon per second per unit length emitted from a point in the discharge is J_{jk}, thus equation (17) may be amended to give

$$J_{jk} = \frac{I_L}{I_s} P_{\Delta\lambda} \frac{\Omega_s A_s}{\Omega_c \Delta x} \qquad (26)$$

where I_L is the photomultiplier current for the line, and I_s is the photomultiplier current for the standard lamp at the wavelength of the line. When the flux ratios are taken the geometric term, $\frac{\Omega_s A_s}{\Omega_c \Delta x}$, will cancel leaving only the ratios of photomultiplier currents and $P_{\Delta\lambda}$ to be evaluated.

There is a set of levels which make transitions in two regions of the spectrum that are so widely separated that no single detector can detect radiation in both regions with the required sensitivity. Some of the levels in this set are those which can make transitions in a favorable region and also to the ground state; the transitions to the ground state are in the vacuum ultraviolet, which we are not able to detect. Some of these elements will be identified later, and discussed in Chapter V. Other elements of this set include the levels of $3p^5 5p$ configuration (this notation will be explained in Chapter III) which make transitions in the visible-near-ultraviolet region and in the infrared at about 1500 nm and longer. This set of levels is sufficiently important to make it desirable to construct an apparatus to measure the flux ratios for these levels.

Since the two regions do not overlap one must measure the flux ratios in each region, then select a line in each region, measure the absolute flux of each line, and then take the ratio of these fluxes. This ratio will establish the scale between the two spectral regions and thus allow one to obtain the missing optical cross sections.

The infrared part of the apparatus is designed around an InAs photovoltatic detector. This detector is designed to operate at liquid nitrogen temperature and thus requires a cryostat. This cryostat must not only cool the detector and provide a window for radiation but also provide good electrical grounding and shielding, and provide a cold shield. The cold shield is designed so that the detector cannot "see" any part of its room temperature surroundings except the cone of light defined by the rest of the optical system. The optical system is shown schematically in Figure 7.

We were able to observe many argon transitions in the infrared with this apparatus, but we could not observe the lines of interest. The effect of this null experiment will be discussed further in Chapter V.

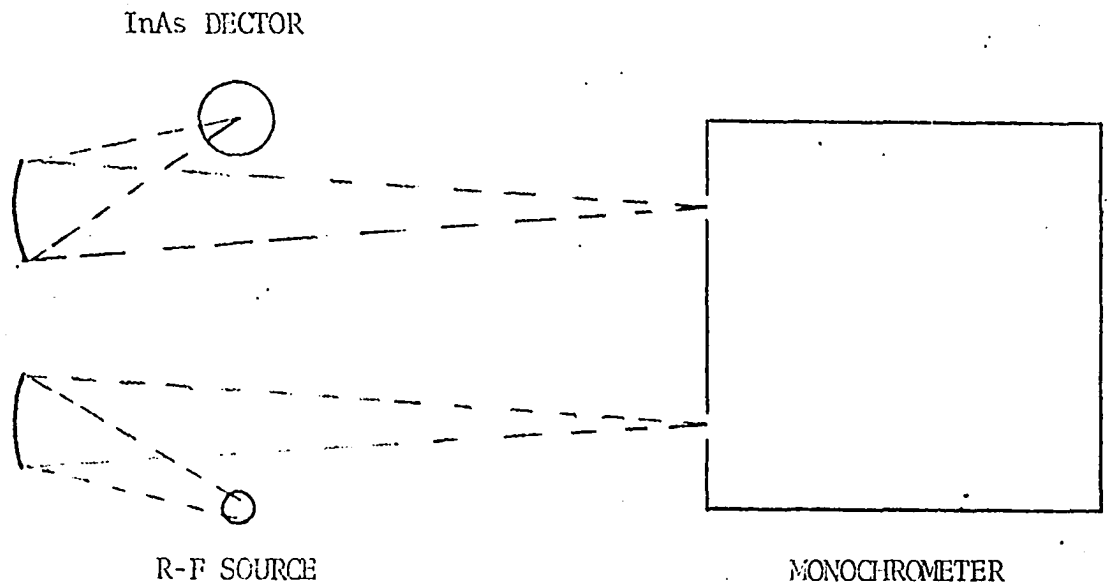

Figure 7. Optical configuration for the infrared flux ratio experiment.

CHAPTER III

STRUCTURE OF ARGON

In this chapter we will discuss some of the relevant aspects of the atomic structure of argon necessary for a clear discussion of argon excitation. First of all, the electron configuration of the ground state target atom is $1s^2 2s^2 2p^6 3s^2 3p^6$, and when the atom is excited it may transform into numerous other configurations. The set of configurations in which one of the outer 3p electrons is excited are much more likely than any of the others. These configurations may be represented as $1s^2 2s^2 2p^6 3s^2 3p^5 n\ell$ where n is the principal quantum number of the excited electron's orbital, and ℓ is the orbital angular momentum of the orbital. It would be a mistake to assume that there is only one excited state for each configuration since there is considerable interaction between the excited electron and the core electrons. This interaction produces several excited states for each configuration, which can be demonstrated by using the L-S coupling scheme, and the configuration $1s^2 2s^2 2p^6 3s^2 3p^5 ns$ as an example. In this case the excited electron gives an ℓ(excited) = 0 and a s(excited) = 1/2, while the core electrons give an ℓ(core) = 1 and a s(core) = 1/2. Now combining these in the usual

way we get an L = 1 and a S = 1 or 0, and these terms represent four states, i.e., $^3P_2$, $^3P_1$, $^3P_0$, and $^1P_1$. If one carries this analysis further to configurations like $3p^5np$ or $3p^5nd$ (the configuration of the core electrons will not be written from now on for convenience) one would find 10 states for the $3p^5np$ and 12 states for the $3p^5nd$ configuration. One must not be tempted to rely on the L-S scheme by its early success in predicting the correct number of states for each configuration, since further analysis shows that the L-S selection rules do not apply to argon transitions. In fact, none of the coupling schemes of the L-S, jj type provide a reasonable description of the structure of argon. There is however a systematic way to describe these excited states.

This description is based on the fact that in argon, and some of the other complex atoms, there is only one good quantum number, J, associated with each of the excited states and since in any configuration there are several states with the same J, another label is needed. For argon these labels are usually chosen to be those used by Paschen, the first researcher to give a systematic account of the argon spectrum. Table 1 gives examples of the configuration, J value, and the Paschen notation for a number of states. The Paschen notation consists of a number, related to the principal quantum number of the excited electron, and a letter, related to the orbital angular momentum of the excited electron. The number is related to the

Table 1. Examples of the number of states in each configuration, the Paschen notation for this state, and its J.

Configuration	Paschen Notation	J
$3p^5 4s$	$1s_2$	1
	$1s_3$	0
	$1s_4$	1
	$1s_5$	2
$3p^5 4p$	$2p_{10}$	1
	$2p_9$	3
	$2p_8$	2
	$2p_7$	1
	$2p_6$	2
	$2p_5$	0
	$2p_4$	1
	$2p_3$	2
	$2p_2$	1
	$2p_1$	0
$3p^5 4d$	$4d_6$	0
	$4d_5$	1
	$4d'_4$	4
	$4d_4$	3
	$4d_3$	2
	$4d_2$	1
	$4d''_1$	2
	$4d'_1$	3
	$4s''''_1$	2
	$4s'''_1$	3
	$4s''_1$	2
	$4s'_1$	1

configuration and principal quantum number by the following rule,

$$P = n-3 \quad \text{for } 3p^5ns \tag{27}$$

$$P = n-2 \quad \text{for } 3p^5np \tag{28}$$

$$P = n \quad \text{for } 3p^5nd \tag{29}$$

where P is the number in the Paschen notation for the state.

Selection rules for this scheme are $\Delta\ell=\pm1$ and $\Delta J=0,\pm1$ and J = 0 to J = 0 transitions are forbidden. It can be seen by examining Table 1 that the $\Delta\ell = \pm1$ can be applied by just looking at the Paschen notation of two states; s_2, s_3, s_4, s_5 are used only for $3p^5ns$, p is used only for $3p^5np$, while d and s_1 are used for states of $3p^5nd$ configurations. The ΔJ rule however can only be applied when J for the two states is know for each state, since there is no general rule for how the letter designations are assigned to states of a particular J.

A schematic for the relative positions, with respect to energy, for the states of several configurations is shown in Figure 8 . Note that states from similar configurations are arranged in the same column so that transitions can only occur between adjacent columns, and that the first group of excited states above the ground state is the $3p^54s$ group not the $3p^53d$ group as one would normally expect.

The relative wavelengths of each allowed group of transitions is very important in determining which states

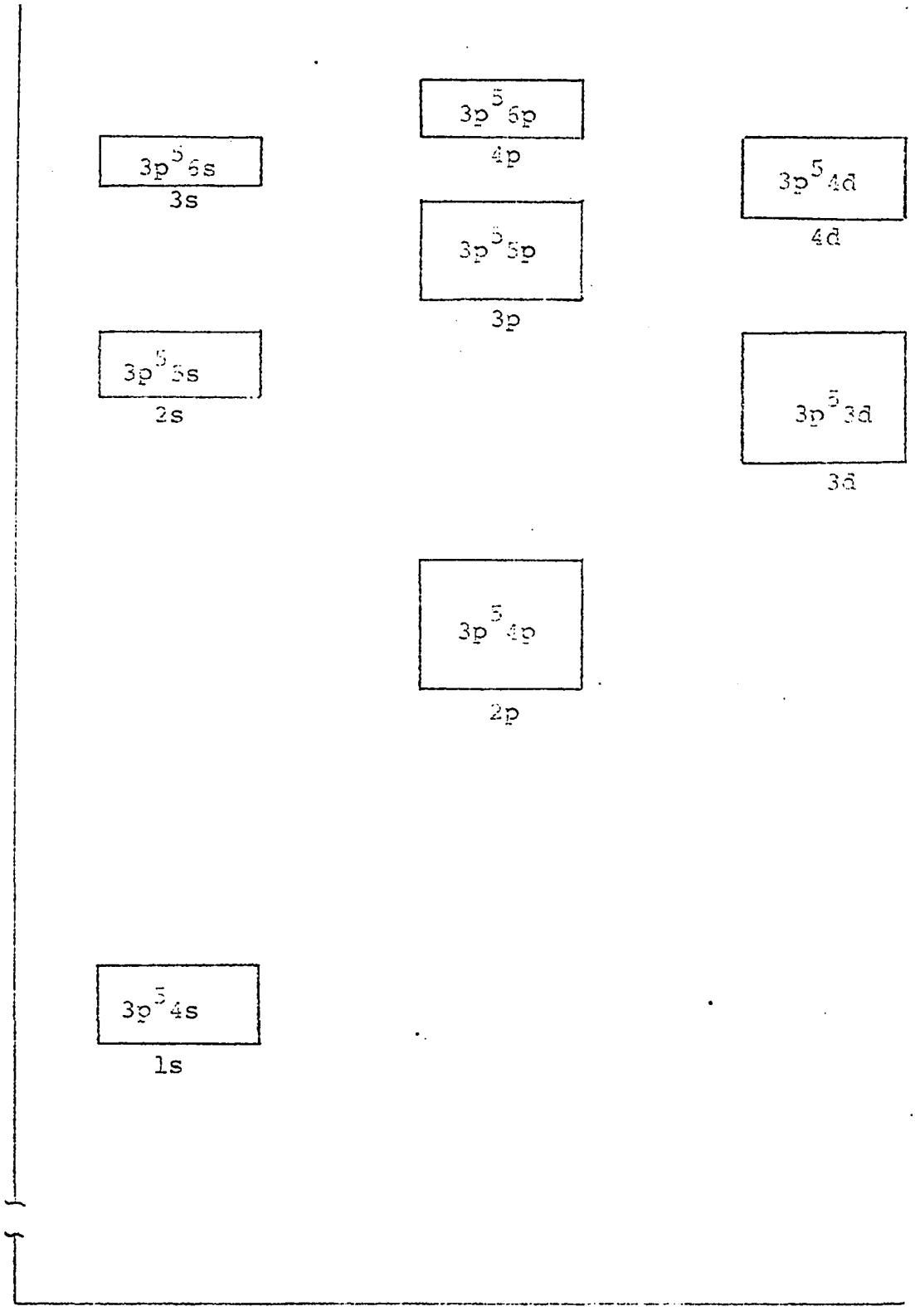

Figure 8. Relative positions of states of several configurations.

Table 2 . Examples of transitions among groups and their respective wavelength ranges. This table should aid in understanding which groups can be studied at this time.

Upper Group		Lower Group		Wavelength
Configuration	Paschen	Configuration	Paschen	Range
$3p^5 4d$	4d	$3p^5 5p$	3p	Infrared
		$3p^5 4p$	2p	Visible-Infrared
$3p^5 5p$	3p	$3p^5 6s$	3s	Infrared
		$3p^5 3d$	3d	Infrared
		$3p^5 5s$	2s	Infrared
		$3p^5 4s$	1s	Ultraviolet-Visible
$3p^5 6s$	3s	$3p^5 4p$	2p	Infrared
$3p^5 3d$	3d	$3p^5 4p$	2p	Infrared
$3p^5 5s$	2s	$3p^5 4p$	2p	Near Infrared

CHAPTER IV

THEORY

In this chapter we will discuss the basic theory of the excitation of argon. The framework of this discussion is built about a theory developed for the excitation of neon by Sharpton et al.[11]

In describing the electronic structure of the atomic state, the one-configuration approximation is used. For a given configuration $3p^5 n\ell$, the Hartree-Fock-Slater self-consistant-field method[4] is applied to compute the one-electron orbitals from which we construct the basis functions of the LS representation. Since the vector coupling between the various spin and orbital angular momenta is of the "intermediate" kind, the wave function of a state (of a given total angular momentum J) is expressed as a linear combination of the LS-eigenfunctions of the same J. The coefficients of the LS-eigenfunctions are determined by means of the method given by Cowan and Andrew [5] in which the values of the spin-orbit coupling constants and the Slater-Condon parameters are chosen so as to yield the best fit to the observed spacing of the energy levels of the configuration.

In discussing the qualitative behavior of electron

excitation of the argon atom, we find it advantageous to express the wave functions of the excited states in the LS-representation. As the excitation properties of a hypothetical LS-state are know from Born-approximation considerations and/or the experimental results of the helium atom, by an appropriate superposition one can make theoretical predictions concerning the shape of the excitation functions and the magnitude of the excitation cross sections for argon, at least on a qualitative level. For instance the four LS-eigenfunctions associated with the $3p^5 4s$ configuration are $\phi(^1P_1)$, $\phi(^3P_0)$, $\phi(^3P_1)$ and $\phi(^3P_2)$, whereas the actual atomic states of argon of this configuration (intermediate coupling) are designated as $1s_2(J=1)$, $1s_3(J=0)$, $1s_4(J=1)$, and $1s_5(J=2)$. Since the total angular momentum J remains a good quantum number, the wave functions of $1s_3$ and $1s_5$ are simply $\phi(^3P_0)$ and $\phi(^3P_2)$ respectively, and those of $1s_2$ and $1s_4$ are linear combinations of $\phi(^1P_1)$ and $\phi(^3P_1)$. One then expects the excitation functions of the $1s_3$ and $1s_5$ states to peak sharply near the threshold, similar to triplet-excitation of helium. For the $1s_2$ and $1s_4$ states, because of the presence of the $\phi(^1P_1)$ component in their wave functions, the excitation functions in general should exhibit a very broad peak characteristic of the dipole-allowed states, and the excitation cross sections should be larger than those of $1s_3$ and $1s_5$ at energies well above the threshold. Exception to the preceeding statement, however, may occur if the coefficient of the $\phi(^1P_1)$ term

in the $1s_2$ or $1s_4$ wave function turns out to be very small. A similar analysis shows that the $2p_9$ state of $3p^5 4p$ and the $4d_6$ and $4d_4$ states of $3p^5 4d$ are purely triplet states with the characteristic narrow-peak excitation functions and that the $4d_5$, $4d_2$, and $4s_1$ states (all J=1) in general may be expected to have broad peaks in their excitation functions.

To gain some insight to the magnitude of the cross sections of excitation from the ground state (g) to a final state (f), let us examine the Coulomb interaction of the six outer electrons of the atom (denoted by subscripts 1-6) with the colliding electron (denoted by subscript 7), or more specifically the coupling potential between the two states concerned, i.e.,

$$V_{fg}(7) = \int \psi_f^* (1,2,\ldots,6)\left[\sum_{j=1}^{6}(1/r_{j7})\right] \psi_i(1,2,\ldots,6)\, d\vec{r}_1 \ldots d\vec{r}_6 . \quad (30)$$

By means of an expansion of the type

$$\frac{1}{r_{17}} = \frac{1}{r_{>k}} \sum_{q=-k}^{k} \frac{4\pi}{2k+1} \left(\frac{r_<^k}{r_>}\right) Y_{kq}^*(\theta_7\phi_7) Y_{kq}(\theta_1\phi_1), \quad (31)$$

it can be shown that for a final state characterized by the configuration $3p^5 n\ell$ and the total angular momentum J, V_{fg} vanish if $J + \ell$ is even. Under the nonexchange Born approximation, such a state would have zero excitation cross section; in other words excitation occurs only through exchange effect and indirect coupling between g and f via some intermediate states. At high energies these effects are in general small compared to that due to non-vanishing direct

coupling, thus one is lead to the general conclusion that within a configuration $3p^5n\ell$, the excitation cross sections of the states with odd values of $J + \ell$ as a whole are larger than those of the group of states with even $J + \ell$ at energies well above the threshold.

In reference to the specific case of the $3p^5np$ configuration, the above rule leads to

$$Q(3p^5np,\ J=0,2) > Q(3p^5np,\ J=1,3)\ . \qquad (32)$$

Following the reasoning given in Ref. 11, one can further expect

$$Q(3p^5np,\ J=0) > Q(3p^5np,\ J=2), \qquad (33)$$

because the coupling potential between the $3p^5np$, $J=0$ state and the ground state ($J=0$) owes its origin to the first term ($k=0$) of the expansion in equation (31), whereas one must proceed to the $k=2$ term of the same expansion in order to obtain non-vanishing coupling of the $3p^5np$, $J=2$ with the ground state. Both equations (32) and (33) pertain to only the "high-energy" region, i.e., energies several times the threshold energy. Likewise for the $3p^5nd$ configuration we have

$$Q(3p^5nd,\ J=1,3) > Q(3p^5nd,\ J=0,2,4), \qquad (34)$$

and

$$Q(3p^5nd,\ J=1) > Q(3p^5nd,\ J=3), \qquad (35)$$

for high energies. The last inequality is based on the

observation that the necessary coupling potentials for excitation of the J = 1 and J = 3 states (of $3p^5nd$) are associated with respectively the k = 1 and k = 3 term of equation (31). It should be emphasized that the interpretation of equations (32)-(35) must be made with some care. For instance equation (33) indicates that the J = 0 states as a group have larger cross sections than the J = 2 state as a group, but does not mean that the cross section of any one of the $3p^5np$, J = 2, states may not be larger than some of the J = 0 states. Possible exception on an individual basis may occur if a J = 0 state, though normally consisting of a superposition of the $^1S_0$ and $^3P_0$ LS-eigenstates, happens to have a very small weighting of the $^1S_0$ component and, as a result, unusually small cross sections. Among the states with even values of J + ℓ for which equation (31) gives no coupling, it was pointed out in Ref. 11 that one may expect the indirect coupling effect to be much weaker for the purely triplet states than for the singlet-triplet mixed ones and therefore smaller excitation cross sections for the former groups. According we may write

$$Q(3p^5np,\ J=1) > Q(3p^5np,\ J=3), \qquad (36)$$

$$Q(3p^5nd,\ J=2) > Q(3p^5nd,\ J=0,4) \qquad (37)$$

Again the two preceeding inequalities, strictly speaking, apply to the states inside the parentheses as a group. In dealing with cross sections of the individual levels, one should be aware of possible exceptions.

CHAPTER V

RESULTS

Section I - Comparison with other Investigators

Measurements of electron excitation cross sections of argon have been reported by Fischer[6] and by Herrman[7] in the 1930's and more recently by Volkova and Devyatov[8] and by Zapesochnyi and Feltsan.[9] We found rather substantial differences in the shape of excitation functions between the results of Herrmann[7] and of this work, and the peak excitation cross section in some cases differ by a factor over two. Likewise our excitation data of the 3p states show significant discrepancy from those of Fischer.[6] Because of the differences in the experimental methods used by Fischer and by Herrmann from ours, no detailed comparison of these three groups of data will be made. Our peak cross sections (apparent) of the 2p states agree to within about 20 per cent with those of Zapesochnyi and Feltsan[9] with the exception of the $2p_4$, $2p_9$, and $2p_{10}$ states where a difference ranging from 40 per cent to a factor of two was found. Compared to the data of Volkova and Devyatov,[8] our peak optical cross sections for a number of 2p→1s lines are in general considerably larger than the corresponding effective cross sections given in Ref. 8.

It may be noted that for detecting the atomic radiation, photographic films were used by Volkova and Devyatov,[8] whereas photoelectric recording was adopted in the work of Zapesochnyi and Feltsan.[9]

For the purpose of comparison of our experimental data with those obtained from other laboratories, we have measured the excitation cross sections of 480.6 nm and 457.9 nm lines of Ar^+, the 585.2 nm and 594.5 nm lines of Ne. In all cases our results agree to within 15 per cent or better with those of Latimer and St. John[10] (Ar^+) and of Sharpton et al[11] (Ne).

Section II - 2p and 3p Families

The optical excitation functions of the ten 2p levels of argon are displayed in Figure 9. Several special features are readily recognizable. The $2p_9$ state, which is a pure $^3D_3$ state, exhibits a narrow excitation function characteristic of a triplet state. The two J = 0 states ($2p_1$ and $2p_5$) have distinctly broader excitation functions than all the others. (The narrow spikes at 20 eV will be discussed in the next paragraph.) In comparing the excitation functions of the J = 0 states with those of the J = 2 states, one may recall that from the theoretical viewpoint, the coupling potentials connecting the ground state with the J = 0 states and with the J = 2 states can be traced to the k = 0 and the k = 2 terms respectively in the expansion of equation (31). For the case of helium the k = 0 terms are

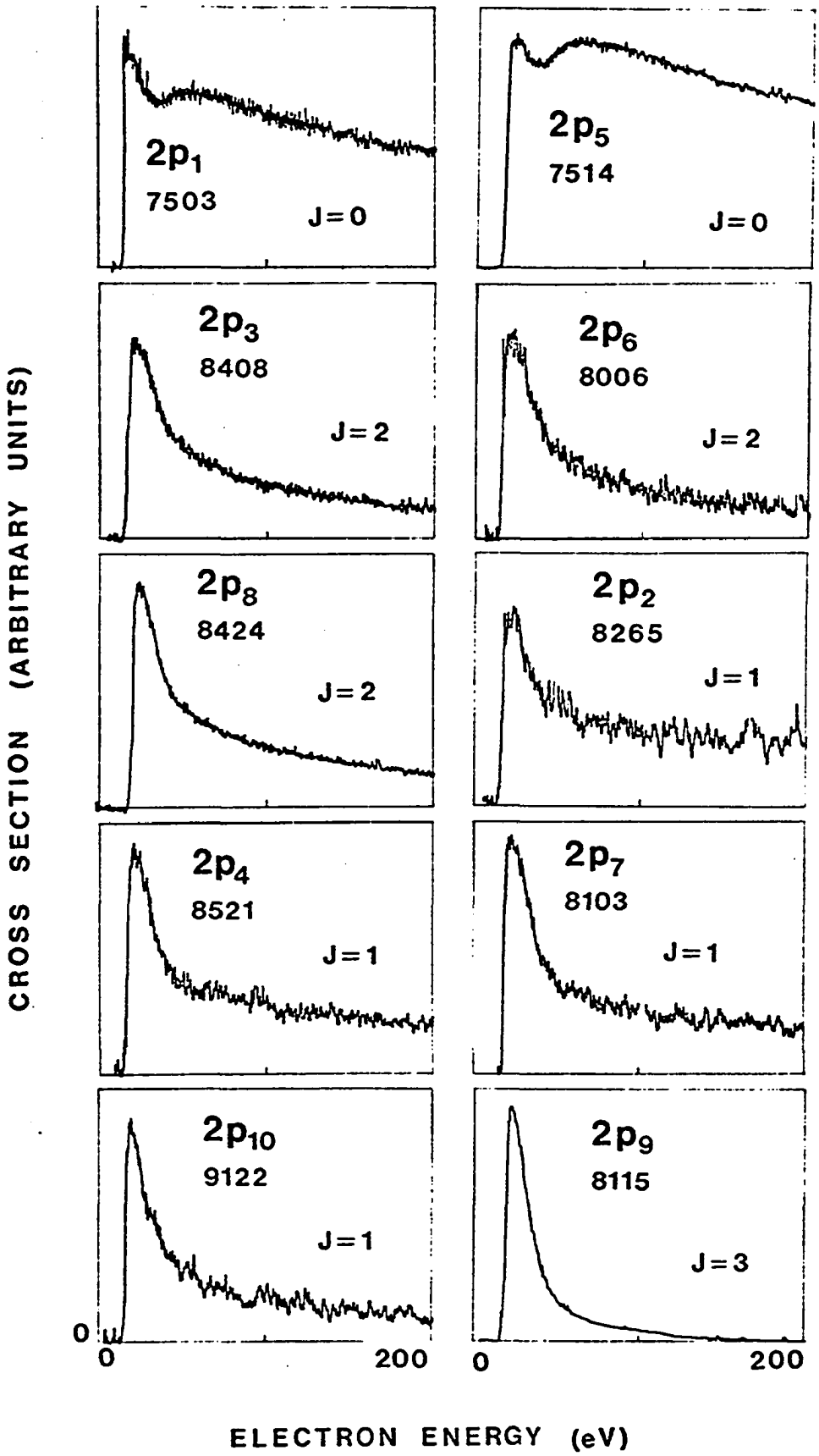

Figure 9. Excitation functions for 2p 1s lines.

responsible for the excitation of the ^1S states and the k = 2 terms for ^1D. Examination of the experimental excitation data of helium shows the ^1S excitation functions to have a slower decline with increasing energy than the ^1D functions. Thus we see a parallel analogy between argon and helium in this respect. As for the J = 1 states, the coupling potentials connecting them with the ground state vanish, and the cross sections are attributed to exchange and indirect coupling effects. The excitation functions would have a very narrow shape if the exchange effect completely dominates the indirect coupling, but become broader as the indirect-coupling effect plays a more important role. We see from the experimental data that the curves of the J = 1 states are much broader than that of the pure triplet state $2p_9$. In fact there appears to be no gross difference between the J = 1 and the J = 2 groups as far as the general width of the excitation functions are concerned except for the $2p_{10}$ which does have a distinctly narrower excitation function than all the other J = 1 members. Thus from a comparison of the shape of the excitation functions, one can recognize the importance of indirect couplings in determing excitation cross sections.

Another interesting feature is that both the $2p_1$ and $2p_5$ curves show a narrow peak at about 20 eV before reaching the broad maximum. The same double-peak feature is also found in the cases of $3p_1$, $3p_5$, $4p_1$, and $4p_5$. One may

wonder if the low-energy narrow peak may be due to cascade from some triplet-like levels. However, the purely triplet states of the $3p^5ns$ and $3p^5nd$ configurations have J = 0,2 and J = 0,4 respectively; none of these states are capable of dipole-radiative cascade to $2p_1$ and $2p_5$ (J = 0). Although some of the J = 1 states (e.g., $4d_5$), which are optically allowed with respect to $2p_1$ and $2p_5$, accidentally have very steep-descending excitation functions (see Section III), it is very unlikely that cascade from such states can account for the sharp peak near the onset of the excitation functions of all the $2p_1$, $2p_5$, $3p_1$, $3p_5$, $4p_1$, and $4p_5$ states. One possible explanation is that the wave functions of the $2p_1$ and $2p_5$ states consist of linear combinations of the LS-eigenfunctions of $^3P_0$ and $^1S_0$, the sharp-peak contribution of the $^3P_0$ component, when added to a rather broad excitation function, produces a noticeable peak near the onset. However, this is merely a speculation as we have not investigated it in any quantitative way.

The optical cross sections of the ten lines exhibited in Figure 9 can be found in Table 3, while the optical cross sections of the other lines at maximum and 100 eV can be found in Table 4. The apparent excitation cross sections are then obtained by using the procedure described in Chapter I, and are listed in Table 5. The flux ratios measured in this experiment for the $3p^54p \rightarrow 3p^54s$ transitions can be found in Table 6, as well as the flux ratios that could be measured from the electron-beam, and ratios of transition probabilities from Ref. 12 (marked NBS). In the case of a discrepancy between our ratios and the

Table 3. Optical cross sections(at maximum and at 100 eV) measured in units of 10^{-19} cm^2.

Transition	λ(nm)	Q_{ij} Max	100 eV
$2p_1$-$1s_2$	750.3	97	64
$2p_5$-$1s_4$	751.4	39	36
$2p_3$-$1s_2$	840.8	96	25
$2p_6$-$1s_4$	800.6	15	3.4
$2p_8$-$1s_4$	842.4	122	32
$2p_2$-$1s_2$	826.5	24	9.7
$2p_4$-$1s_2$	852.1	23	7.0
$2p_7$-$1s_4$	810.3	50	13
$2p_{10}$-$1s_5$	912.2	150	27
$2p_9$-$1s_5$	811.5	260	11

Table 4. Optical cross section for the 2p→1s lines at 100 eV in units of 10^{-19} cm^2. Dashes indicate no transition possible.

	$2p_1$ J=0	$2p_2$ J=1	$2p_3$ J=2	$2p_4$ J=1	$2p_5$ J=0	$2p_6$ J=2	$2p_7$ J=1	$2p_8$ J=2	$2p_9$ J=3	$2p_{10}$ J=1
$1s_2$ J=1	64	9.7	25	7.0	0	5.4	.83	4.4	--	.29
$1s_3$ J=0	--	4.3	--	5.9	--	--	2	--	--	2.2
$1s_4$ J=1	0	.92	8.7	.013	36	3.4	13	32	--	15
$1s_5$ J=2	--	3.1	4.3	.19	--	17	2.6	16	11	27

Table 5. Experimental values of the apparent and level cross sections of the 2p states at 100 and 200 eV and comparison with the theoretical level cross sections in units of $10^{-19}cm^2$.

		100 eV			200 eV		
States	J	Expt. App. Q	Expt.[a] Level Q	Theor. Level Q	Expt. App. Q	Expt.[a] Level Q	Theor. Level Q
$2p_1$	0	64	63	82.4	48	48	43.1
$2p_5$	0	36	35	18.2	28	28	9.6
$2p_3$	2	38	33	6.0	22	19	3.2
$2p_6$	2	26	24	7.4	14	13	4.0
$2p_8$	2	52	48	6.4	27	24	3.4
$2p_2$	1	18	16		12	11	
$2p_4$	1	13	11		8.8	7.8	
$2p_7$	1	18	17		12	11	
$2p_{10}$	1	44	39		16	13	
$2p_9$	3	11	9	0.33	2	2	0.04

[a]Corrections for cascade from the 2s and 3d state were not made because of lack of experimental data.

Table 6 . Flux ratios measured in this experiment for the $3p^5 4p \rightarrow 3p^5 4s$ transitions, and transition probability ratios from Ref. [12].

		$2p_1$ J=0	$2p_2$ J=1	$2p_3$ J=2	$2p_4$ J=1	$2p_5$ J=0	$2p_6$ J=2	$2p_7$ J=1	$2p_8$ J=2	$2p_9$ J=3	$2p_{10}$ J=1
$1s_2$	R-F	1	1	1	1	0	.32	.064	.14	--	.011
	Beam			1	1					--	
J=1	NBS	1	1	1	1	0	.24	.041	.069	--	.012
$1s_3$	R-F	--		--	.84	--	--	.15	--	--	.088
	Beam	--		--	.73	--	--		--	--	
J=0	NBS	--	.75	--	1.3	--	--	.10	--	--	.055
$1s_4$	R-F		.095	.34	.0019	1	.40*	1	1	--	.58
	Beam			.35			.20			--	.54
J=1	NBS		.12	.35	.0017	1	.19	1	1	--	.28
$1s_5$	R-F	--	.32	.014	.027	--	1		.51	1	1
	Beam						1				1
J=2	NBS	--	.40	.162	.044	--	1	.21	.41	1	1

* The ratio from the beam was used, since it is the most reliable source.

were not made in our data. In other words the level cross sections of the $2p_{10}$ at 200 eV and of $2p_3$, $2p_4$, $2p_9$ at both 100 and 200 eV given in Table 5 may represent an overestimation by as much as 25-30 per cent.

From Table 5 it is seen that with the exception of $2p_{10}$ state, all the even-J states of the ^2p group have larger cross sections than do the odd-J ones at 100 and 200 eV. The cross sections of the $2p_{10}$ decreases very rapidly with energy. Thus at 100 eV the $2p_{10}$ cross section is well above those of $2p_3$ and $2p_6$, but becomes equal to the $2p_6$ value (the smallest of all J = 2 states) when the incident energy is raised to 200 eV. With increasing incident energies, one may expect the $2p_{10}$ cross sections to drop below those of all the J = 2 states. Among the even-J states, the cross sections of the J = 0 states ($2p_1$ and $2p_5$) are larger than those of the J = 2 states ($2p_3$, $2p_6$, $2p_8$) at 200 eV, although at 100 eV the $2p_8$ cross section exceeds the $2p_5$ value. For the states with odd values of J, the purely triplet $2p_9$ state (J = 3) has lower cross sections than the J = 1 states. These results are in good agreement with the predictions of the theoretical considerations given in Chapter IV.

The theoretical cross sections of the J = 0 and J = 2 states calculated by means of the Born approximation, by Fajen[15], are included in Table 5. For the J = 1 states the use of the Born approximation (with Ochkur's modification) is unrealistic because the effects of indirect coupling

are not taken into consideration. For this reason no theoretical cross sections of the J = 1 states are given. While the theoretical cross sections of the J = 0 states agree reasonable well with experiment, a discrepancy of a factor of 3 to 8 is seen between theory and experiment for the J = 2 states. This discrepancy is of comparable magnitude to the corresponding one for Ne. The Ochkur modification of the Born approximation was employed to calculate the excitation cross sections of the purely triplet state $2p_9$. The theoretical values are found to be more than an order of magnitude smaller than the experimental data.

We have measured the excitation functions of all the 3p states except $3p_7$ and $3p_3$. The two stronger lines of the $3p_7 \rightarrow 1s$ group (427.2 nm and 416.4 nm) are contaminated by Ar^+ lines at nearly the same wavelengths, and the two other lines are too weak to measure in our apparatus. As for the $3p_3$ state, all the three allowed $3p_3 \rightarrow 1s$ lines have neighboring lines (from the $3p_2$ state) within 0.2 nm. The shape of the excitation functions of the eight 3p states in Figure 10 are similar to their counterpart in the 2p series. The ratios of the transition probabilities for the $3p \rightarrow 1s$ lines were measured using the r-f discharge, and can be found in Table 7, along with the ratios that could be measured in the electron-beam, and ratios from data in Ref. 12 (marked NBS). In case of discrepancy we always used our own ratios in preference to the ones from Ref. 12 Only in the case of the $3p_4$ and $3p_8$ levels did we use ratios

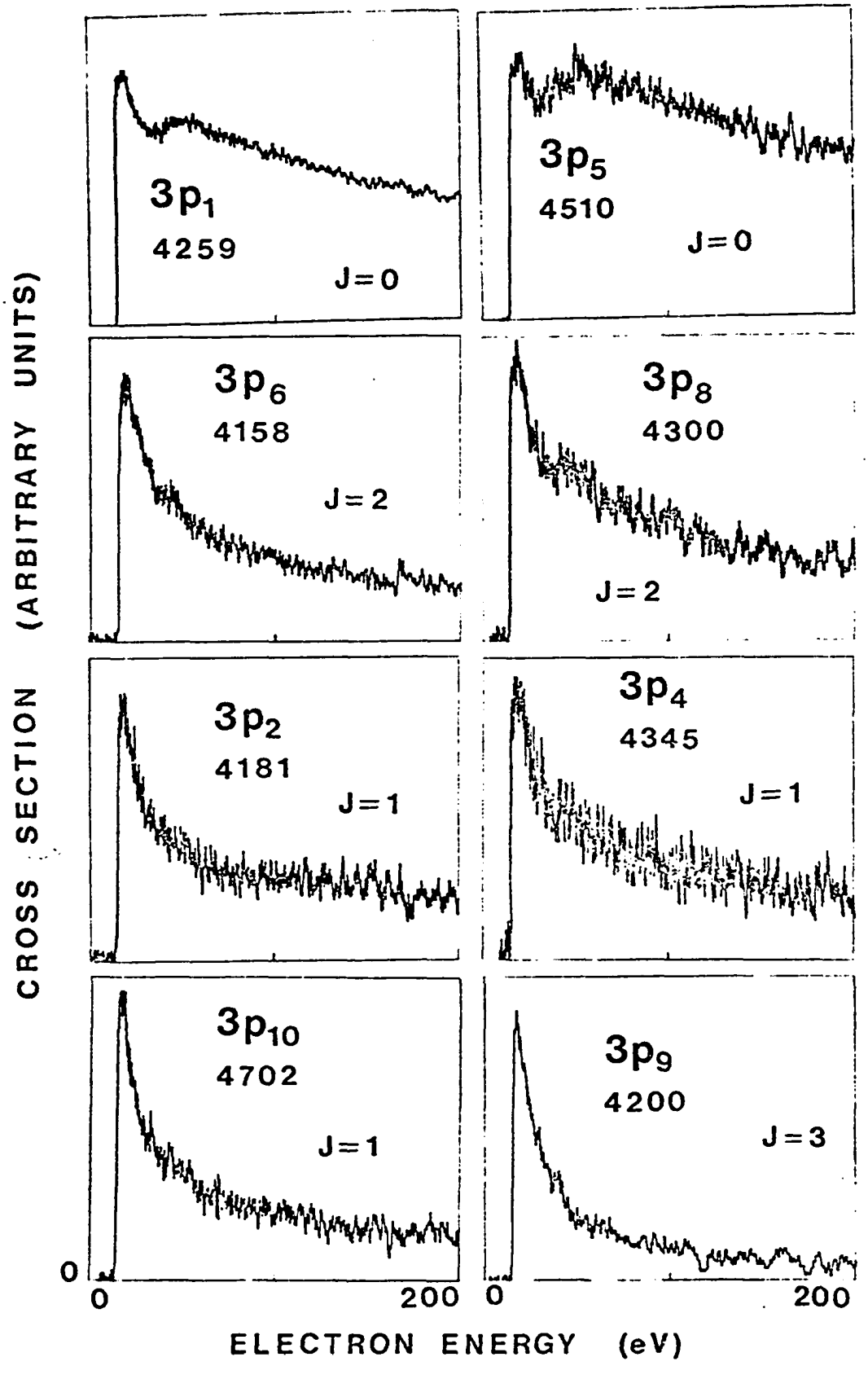

Figure 10. Excitation functions for 3p→1s lines.

Table 7 . Flux ratios measured in this experiment for the $3p^5 5p \rightarrow 3p^5 4s$ transitions, and transitions probability ratios from Ref. [12].

		$3p_1$ J=0	$3p_2$ J=1	$3p_3$ J=2	$3p_4$ J=1	$3p_5$ J=0	$3p_6$ J=2	$3p_7$ J=1	$3p_8$ J=2	$3p_9$ J=3	$3p_{10}$ J=1
$1s_2$	R-F	1	.69	1		.35	.003	.12	.11	--	1
	Beam					.38					
J=1	NBS	1	.67	1	.56	.44	.003	.12	.11	--	1
$1s_3$	R-F	--	1	--		--	--	.01	--	--	.82
	Beam										
J=0	NBS	--	1	--	1	--	--	.01	--	--	.75
$1s_4$	R-F	.003	.088	.73		1	.20	1	1	--	.14
	Beam						.19	1			
J=1	NBS		.076	.58	.048	1	.23	1	1	--	.12
$1s_5$	R-F	--	.74	.12		--	1	.36		1	1
	Beam						1	.34			
J=2	NBS	--	.81	.10		--	1	.35	.65	1	1

from Ref. 12 , since we could not resolve $3p_4 \rightarrow 1s_3$ (419.1 nm) and $3p_8 \rightarrow 1s_5$ (419.0 nm). The same ratios for the 3p→2s and 3p→3d lines could not be measured because the lines for these two groups are in the infrared at wavelengths greater than ∿1500 nm, where our sensitivity is much lower than our sensitivity in the visible region. One can argue that the contribution of these transitions should be negligible since the transition probability of a line is directly proportional to the cube of the frequency of the emitted radiation and since the 3p→1s lines, in the 360 nm to 470 nm, range have a much higher frequency than the 3p→2s or 3p→3d lines, one would expect to be able to neglect the transition probabilities for the infrared groups with respect to the 3p→1s group. This argument, however, tacitly assumes that the dipole matrix element for the 3p→2s or 3p→3d transitions are about the same size as the dipole matrix element for the 3p→1s transitions, which is not necessarily true. In fact the 3p→2s or 3p→3d dipole matrix element may grow sufficiently to compensate for the decrease in frequency, and thus make the contribution of these infrared groups of lines significant and still be consistant with our null infrared experimental results. Other workers, Wiese et al[13] have observed some of these lines and were able to assign transition probabilities to them. One of these authors[14] indicated that the lines observed by them represent the lower limit of their sensitivity and thus the transition probabilities that they assign must be the upper limit for all lines in the infrared group starting on the $3p_2$

and $3p_9$ levels. A comparison of the magnitudes of the infrared transitions and transitions from the same levels in the 3p→1s group is given in Table 8.

Table 8 indicates that the infrared transitions make a significant contribution to the apparent cross section of the $3p_9$ state, and since the contribution to the apparent cross section of this state from these levels is apparently greater than the $3p_9 \rightarrow 1s_5$ contribution, there is considerable doubt about its apparent cross section.

In the $3p_2$ case, however, the one reported infrared transition only makes about a 6 per cent contribution to its apparent cross section and the other nonreported lines make even a smaller contributions. The $3p_2$ apparent cross section should be viewed as fairly reliable.

As far as the other 3p states are concerned the absence of any reported infrared transitions tend to make them all appear to be reliable, but not as reliable as the 2p's.

The optical cross section for the 3p→1s lines displayed in Figure 10 can be found in Table 9, the optical cross sections for the other lines can be found in Table 10, and the experimental and theoretical cross sections are given in Table 11. The absence of the $3p_3$ and $3p_7$ have been explained previously. All of these apparent cross sections have been calculated on the basis of the 3p→1s experimental flux ratios including the $3p_9$ and $3p_2$ levels. The apparent cross sections should be expected to obey the same rules as

Table 8. Comparison of the transition probabilities for the 3p→1s group and the transition probabilities of the 3p→3d transitions reported by Wiese et al[13].

Upper State	J	Lower State	J	Transition Probability (10^8 sec^{-1})
$3p_2$	1	$1s_2$	1	.00387
		$1s_3$	0	.0058
		$1s_4$	1	.000438
		$1s_5$	2	.00467
		$3d_3$	2	.00098
$3p_9$	3	$1s_5$	2	.0103
		$3d'_4$	4	.0119
		$3d_3$	2	.00085

Table 9. Optical cross sections (at maximum and at 100 eV) measured in units of 10^{-19} cm^2.

Transition	λ(nm)	Q_{ij} Max	100 eV
$3p_1$-$1s_2$	425.9	4.3	2.8
$3p_2$-$1s_3$	418.2	.9	.29
$3p_4$-$1s_2$	434.5	.6	.19
$3p_5$-$1s_2$	451.1	2.4	2
$3p_6$-$1s_5$	415.9	.33	.08
$3p_8$-$1s_4$	430.0	.78	.31
$3p_9$-$1s_5$	420.1	6.3	.82
$3p_{10}$-$1s_2$	470.2	.33	.08

Table 10. Optical cross sections at 100 eV for the $3p \rightarrow 1s$ lines in units of 10^{-19} cm^2.

	$3p_1$ J=0	$3p_2$ J=1	$3p_3$ J=2	$3p_4$ J=1	$3p_5$ J=0	$3p_6$ J=2	$3p_7$ J=1	$3p_8$ K=2	$3p_9$ J=3	$3p_{10}$ J=1
$1s_2$ J=1	2.9	.2		.19		.0002		.03	--	.08
$1s_3$ J=0	--	.29	--	.34	--	--		--	--	.06
$1s_4$ J=1	.009	.003		.002		.02		.31	--	.01
$1s_5$ J=2	--	.21			--	.08		.11	.82	.08

Table 11. Experimental values of the apparent excitation cross sections and the theoretical level cross sections (by the Born approximation) at 100 and 200 eV in units of 10^{-19} cm^2.

		100 eV		200 eV	
States	J	Expt. App. Q	Theor. Level Q	Expt. App. Q	Theor. Level Q
$3p_1$	0	2.8	15.1	2.0	8.0
$3p_5$	0	7.6	12.6	5.6	6.7
$3p_3$	2		2.1		1.1
$3p_6$	2	.12	1.3	.08	0.69
$3p_8$	2	.55	2.5	.32	1.3
$3p_2$	1	.73		.50	
$3p_4$	1	.56		.36	
$3p_7$	1				
$3p_{10}$	1	.24		.16	
$3p_9$	3	.08	.11	.05	.014

the 2p states. However the pattern is complicated by the fact that one of the J = 2 levels, the $3p_3$ is missing and the $3p_8$ cross section appears to fall too fast from 100 to 200 eV, and the J = 1 states do not fall fast enough resulting in the case that the 3p (J = 1) are of the same size as the $3p_8$ and larger than the $3p_6$. However, in the case of the 2p (J = 1) states a strong pressure dependence of the excitation function was found, but in the 3p case the lack of intensity did not allow us to observe this pressure dependence, perhaps at lower pressures this problem would not exist.

The theoretical cross sections for the J = 0 and J = 2 states calculated by means of the Born approximation, by Fajen, are included in Table 9. The cross sections for the J = 1 states are not given for the same reasons as the 2p J = 1's. There is a discrepancy of a factor of 1.2 to 8 between the theoretical and experimental cross sections for the J = 0, and J = 2 states which is about the discrepancy for the J = 2 states of the 2p's. The pure triplet J = 3 state, calculated by means of the Ochkur modification to the Born approximations, is a factor of 32 smaller than the experimental value.

Section III - 4d Family

The optical excitation functions of nine of the twelve states of the $3p^5 4d$ configurations display in Figure 11 and

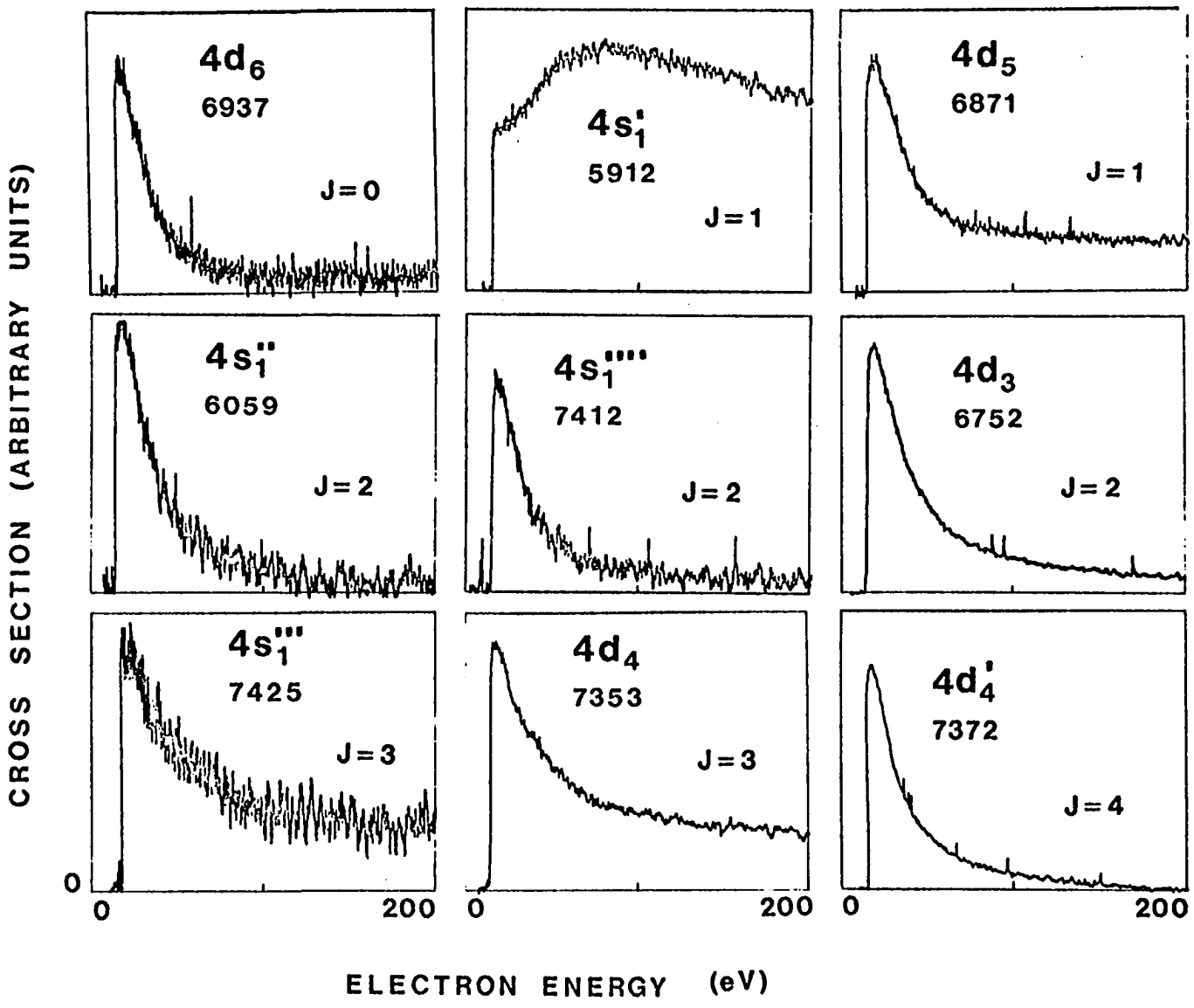

Figure 11. Excitation functions for 4d[3]y Lines.

Table 12. Optical cross sections for the 4d→2p lines (at maximum and at 100 eV) measured in units of 10^{-19} cm^2.

Transition	λ(nm)	Q_{ij} Max	100 eV
$4s'_1-2p_{10}$	591.2	2.2	2.1
$4d_5-2p_{10}$	687.1	5.5	1.4
$4d_4-2p_8$	735.3	5.0	1.6
$4s'''_1-2p_3$	742.5	1.1	0.37
$4d_3-2p_{10}$	675.2	8.3	1.1
$4s''_1-2p_{10}$	605.9	1.1	0.10
$4s''''_1-2p_4$	741.2	1.6	0.17
$4d_6-2p_{10}$	693.7	3.0	0.23
$4d'_4-2p_9$	737.2	23	1.5

Table 13. Optical cross sections of the 4d→2p lines at 100 eV in units of 10^{-19} cm^2. Dashes indicate no transition is possible.

	$2p_1$ J=0	$2p_2$ J=1	$2p_3$ J=2	$2p_4$ J=1	$2p_5$ J=0	$2p_6$ J=2	$2p_7$ J=1	$2p_8$ J=2	$2p_9$ J=3	$2p_{10}$ J=1
$4d_4$ J=3	--	--	0	--	--	.11	--	1.6	.18	--
$4s'''_1$ J=3	--	--	.37	--	--	.16	--	.41	.13	--
$4d_3$ J=2	--	0	0	0	--	0	.068	0	.58	1.1
$4s''_1$ J=2	--	.07	.1	.01	--	.05	.05	0	.06	.1
$4s''''_1$ J=2	--	.08	0	.17	--	.1	.06	.65	.003	.05
$4d_6$ J=0	--	0	--	0	--	--	.06	--	--	.23
$4d'_4$ J=4	--	--	--	--	--	--	--	--	1.5	--

the optical excitation cross sections may be found in Table 12 for the lines in Figure 11; the other optical cross sections can be found in Table 13; spectral lines originating from the three states ($4d_2$, $4d_1''$, and $4d_1'$) are too weak to detect in our collision apparatus. The J = 1 states of the $3p^5nd$ configuration are expected to give rise to very broad excitation functions typical of the dipole-allowed states. The experimental data of the $4d_5$ state, however, are in contradiction with our expectation (Figure 11). The explaination lies in the wave function of the specific state concerned. Within the $3p^5nd$ configuration of a state with J = 1 consists of a superposition of three LS-eigenstates, i.e., $^1P_1$, $^3P_1$, and $^3D_1$, and our intermediate coupling calculations give the coefficients of these three LS-components in the wave function of the $4d_5$ state as 0.120, -0.975, and 0.186 respectively. The contribution to the excitation function of the $4d_5$ state from the $^1P_1$ component, which is responsible for the broad peak, is overshadowed by that from $^3P_1$, resulting in a triplet-like curve.

The $4d_6$ and $4d_4'$ are both pure triplet states ($^3P_0$ and $^3F_4$ respectively), and do indeed exhibit the usual narrow excitation functions. It is interesting to note that the three J = 2 states ($4s_1''$, $4d_3$, $4s_1''''$) have considerable narrower excitation functions than do the J = 3 states. In particular the excitation functions of the $4s_1''$ and $4s_1''''$ states have about the same shape as those

of the purely triplet states. We may recall from the general theory described in Chapter IV that the direct potential coupling of the ground state with the J = 2 states of the $3p^5nd$ configuration vanishes, and excitation of the latter states is caused by exchange and indirect-coupling effects. Exchange effect alone would give rise to a triplet-like excitation function, and inclusion of indirect coupling has the result of broading the curve. The experimental data in Figure 11 are suggestive of relatively small indirect-coupling effect on the cross sections of the $4s_1''$, and $4s_1''''$ states, but appreciable larger for $4d_3$. However, even with the aid of indirect coupling the excitation functions of the J = 2 states do not turn out to be as broad as those of the J = 3 states for which direct coupling with the ground state exists through the k = 3 term of equation (31). This is in contrast to our observations for the 2p group where the J = 1 states (which have no direct potential coupling with the ground state and therefore are the counterpart of the J = 2 states of the 4d group) and the J = 2 states (which connect directly with the ground state corresponding to the $3p^54d$, J = 3 states) have excitation functions of very similar shape.

The ratios for the $3p^54d \rightarrow 3p^54p$ transitions are displayed in Table 14. In this set of data the electron-beam could only detect, at most, one transition from each level so no flux ratios could be obtained from the electron-beam.

Table 14. Flux ratios measured in this experiment for the $3p^5 4d \rightarrow 3p^5 4p$ transitions, and transition probability ratios from Ref.12.

		$2p_1$ J=0	$2p_2$ J=1	$2p_3$ J=2	$2p_4$ J=1	$2p_5$ J=0	$2p_6$ J=2	$2p_7$ J=1	$2p_8$ J=2	$2p_9$ J=3	$2p_{10}$ J=1
$4d_6$	R-F	--	.40	--	.078	--	--	.29	--	--	1
J=0	NBS	--	.029+	--	.029+	--	--	.36	--	--	1
$4d_5$	R-F					.33	.31		.49	--	1
J=1	NBS		.059	.17			.33		.1	--	1
$4s_1''''$	R-F		.73		1		.56	.33	.31	.022	.31
J=2	NBS		.48		1		.56	.46	.39	.059	.49
$4d_3$	R-F		.0049	.0108	.0001		.0099	.045		.53	1
J=2	NBS		.71+	.66+	.62+		.45+	.617		.14	1
$4s_1''$	R-F										
J=2	NBS		.64	1	.15		.53	.55		.62	.90

+ indicates the ratios are upper limits.

Table 14. Flux ratios measured in this experiment for the $3p^5\ 4d \rightarrow 3p^5 4p$ transitions, and transition probability ratios from Ref. 12.

		$2p_1$	$2p_2$	$2p_3$	$2p_4$	$2p_5$	$2p_6$	$2p_7$	$2p_8$	$2p_9$	$2p_{10}$
		J=0	J=1	J=2	J=1	J=0	J=2	J=1	J=2	J=3	J=1
$4d_4$	R-F	--	--		--	--	.071	--	1		--
J=3	NBS	--	--	.25	--	--	.066	--	1	.11	--
$4s_1'''$	R-F	--	--		--	--		--	.64		--
J=3	NBS	--	--	1	--	--	.44	--	.044	.34	--

In the case of the $4d_6$ and $4d_3$ levels upper limits were set on some of the ratios (indicated by a $^+$). For the $4s_1'$' level the only non-contaminated line was the $4s_1'' \rightarrow 2p_{10}$ (605.9 nm) so NBS ratios were used exclusively. In all other cases the flux ratios we measured were used.

The principal depopulation mechanism of the $4s_1'$ state is expected to be the transition to the ground state (83 nm). Since our experimental apparatus is not equipped to handle vacuum ultraviolet radiation, we are unable to determine the apparent excitation cross sections of the J = 1 states. The other 4d states make radiative transitions to 2p and 3p. The 4d→2p lines are in the spectral region of 590-910 nm; their relative intensities were readily determined from our discharge experiment. However, we are not able to observe any of the 4d→3p lines (above 2500 nm). In view of their long wavelengths it is probable that the 4d→3p lines in general have smaller transition probabilities than the 4d→2p lines, and in the absence of experimental data on the transition probabilities of the 4d→3p lines, we shall neglect them in computing the branching ratios in equation (11). The apparent excitation cross sections of the 4d states as given in Table 15 are therefore subject to a higher degree of uncertainty than those of the 2p states.

Determination of the cascade contribution to the 4d states is again complicated by the fact that all the transitions terminating at 4d have frequencies in the infrared region. Nevertheless, to ascertain the importance of the

Table 15. Experimental values of the apparent excitation cross sections of the 4d states at 100 and 200 eV and the theoretical level cross sections in units of 10^{-19} cm^2.

States	J	100 eV		200 eV	
		Expt. App. Q	Theor. Level Q	Expt. App. Q	Theor. Level Q
$4d_4$	3	1.9	1.6	1.3	0.82
$4s_1'''$	3	1.1	3.4	0.8	1.7
$4d_3$	2	1.8		0.8	
$4s_1''$	2	0.4		<0.1	
$4s_1''''$	2	0.5		$\leq$0.3	
$4d_6$	0	0.3	0.11	<0.3	0.013
$4d_4'$	4	1.5	0.31	<0.1	0.039

cascade from the 4p state, we have examined the optical excitation cross sections of the 4p→1s transitions. The only lines from this group, which we can detect in our electron-beam experiment, originate from $4p_1$ and $4p_5$ (both J = 0) which cascade only to the J = 1 states of $3p^5 4d$, but not to the states listed in Table 13. For all the other 4p→1s (except $4p_1$ and $4p_5$) lines we can place an upper limit on the cross section at 100 eV as 3×10^{-21} cm^2. Of course we do not have a good estimate of the transition probabilities of 4p→1s relative to 4p→4d. In view of the fact that $\ell \rightarrow \ell+1$ cascade is usually less favorable than $\ell \rightarrow \ell-1$ and in view of the low frequencies of the 4p→4d transitions, it is not likely that these lines have sufficiently large transition probabilities to make significant cascade contributions to the 4d states. Another source of cascade is from the $3p^5 nf$ states; however, we are unable to detect any emmission lines from these states on our excitation experiment. Our theoretical calculations give excitation cross sections of all three $4p^5 4f$, J = 2 states as about 1×10^{-20} cm^2 at 100 eV and much smaller (by an order of magnitude or more) cross sections for all other members of the same configuration. Each $4p^5 4f$, J = 2 state may cascade to a total of 14 states of the $4p^5 3d$ and $4p^5 4d$ configurations, thus one would expect the 4f-cascade contribution to the apparent cross sections of the 4d states listed in Table 15 to be quite small. For the reasons

described in this paragraph we shall take the apparent excitation cross sections of Table 15 as being approximately equal to the level cross sections.

Inspection of Table 15 reveals that the experimental cross sections for the J = 3 states as a group are larger than the ones for the even-J states as expected from theoretical grounds. When an examination of each individual state is made, we do notice an exception in that the $4d_3$ cross section is larger than the $4s_1'''$ one at 100 eV. However, at 200 eV the cross sections of these two states become equal to each other, thus at higher energies we expect the $4d_3$ cross sections to drop below $4s_1'''$ since the excitation function of the $4d_3$ state declines more steeply with energy than its $4s_1'''$ counterpart. Among the even-J we again find good accordance between theory and experimental results in that the J = 2 states collectively have larger cross sections than do the two purely triplet states (J = 0,4) at 200 eV. Comparison on an individual basis in this case is made difficult because of the large degree of uncertainty of the cross sections for most of the even-J states at 200 eV. Of some interest is the observation that the $4d_3$ state has a much larger cross section than the other two J = 2 states in Table 15. Since the J = 2 states do not couple directly with the ground state through coulomb interaction, our experimental data here suggest that the indirect-coupling effect

is much more prominent in the $4d_3$ state than in $4s_1''$ and $4s_1'''$. It may be recalled that the same conclusion was obtained by consideration of the shape of the excitation functions.

Theoretical level cross sections calculated by the Born approximation (with Ochkur's modification for the purely triplet states) are included in Table 15. The overall agreement between the theoretical and experimental values is seen to be reasonable satisfactory.

Section IV - 3s Family

The optical excitation functions of the four 3s states as shown in Figure 12. As may be expected, narrow excitation functions are found for the purely triplet states $3s_3$ and $3s_5$, whereas the $3s_2$ and $3s_4$ (J = 1) show the broader peak characteristic of the dipole-allowed states. No attempt has been made, however, to evaluate the apparent excitation functions due to the lack of experimental data of the transition probabilities of the 3s→3p lines and especially the emmission lines from $3s_2$ and $3s_4$ to the ground state.

Section V - nd_4'

It is of interest to see if the pure triplet J = 0 and J = 4 states introduced in Section III maintain their narrow excitation function for $3p^5nd$ configurations (n>4).

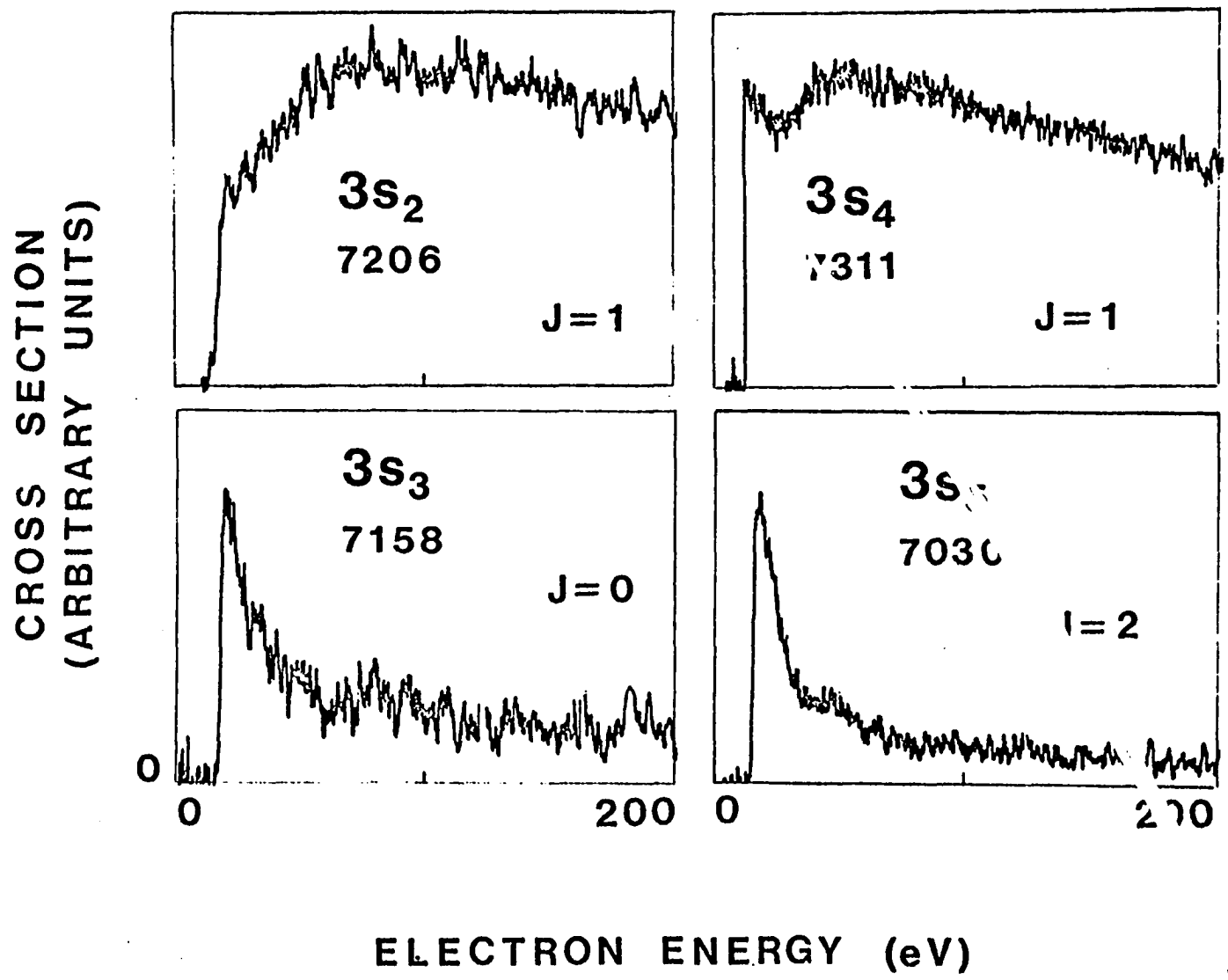

Figure 12. Excitation functions for 3s→2p lines.

One finds that for n>4 the nd_6 (J = 0) transitions can not be observed while the nd_4' (J = 4) states can be observed. The reason for this is that the nd_4 (J = 4) states can only make transitions to the np J = 3 states, predominately to the $2p_9$ (J = 3) state, while the population of the nd_6 (J = 0)'s is divided among all of the np J = 1 states thus reducing the flux for each of these lines. The excitation functions for $5d_4'$ and $6d_4'$ are shown in Figure 13, and the excitation functions for the $7d_4'$ and $9d_4'$ are shown in Figure 14. The $8d_4' \rightarrow 2p_9$ transition (506.0 nm) is contaminated by Ar^+ line at 506.1 nm and is not shown for that reason. All of these nd_4' states maintain the narrow pure triplet excitation functions as n increases.

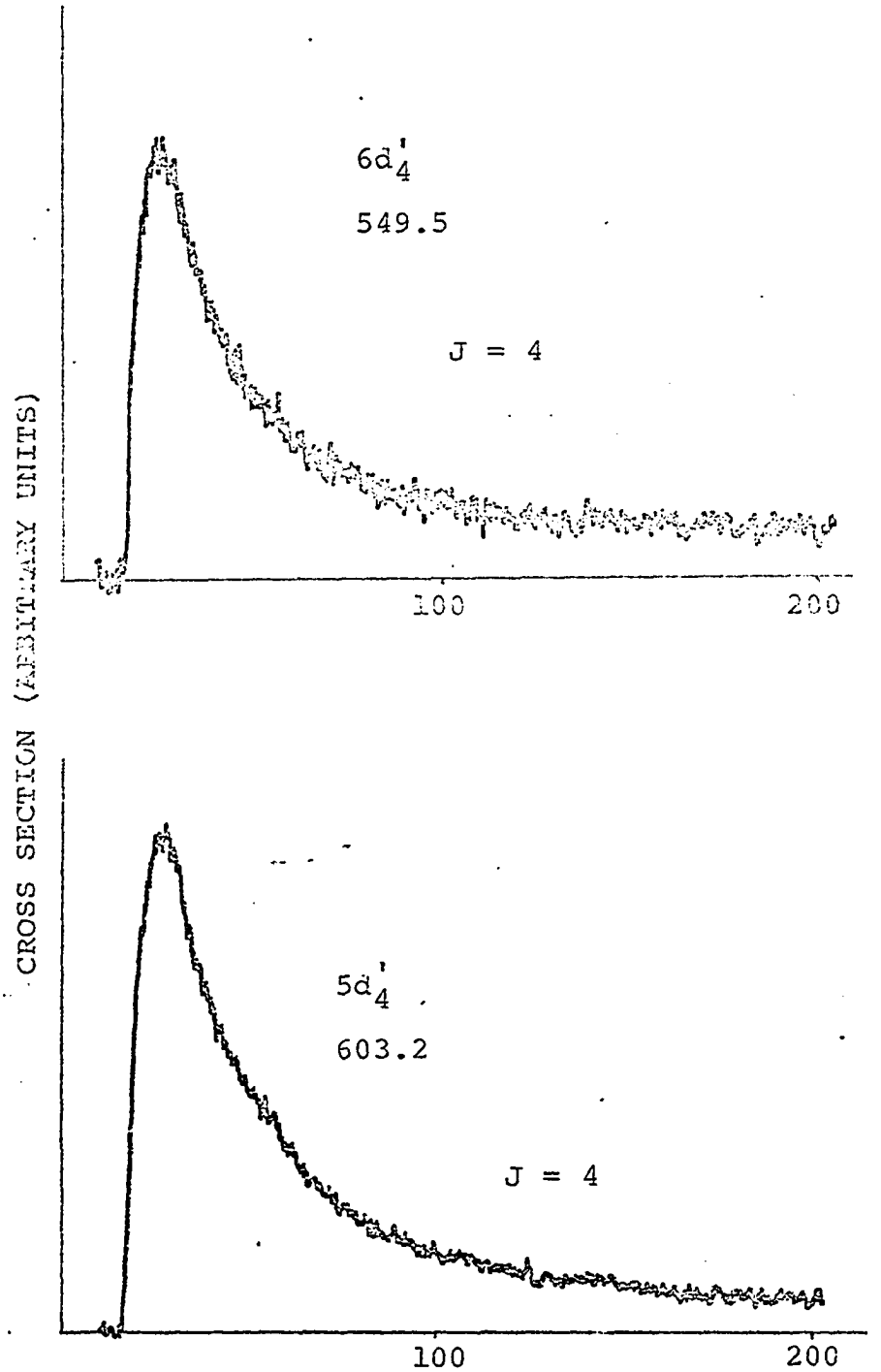

Figure 13. Excitation functions for $5d_4'$ and $6d_4'$.

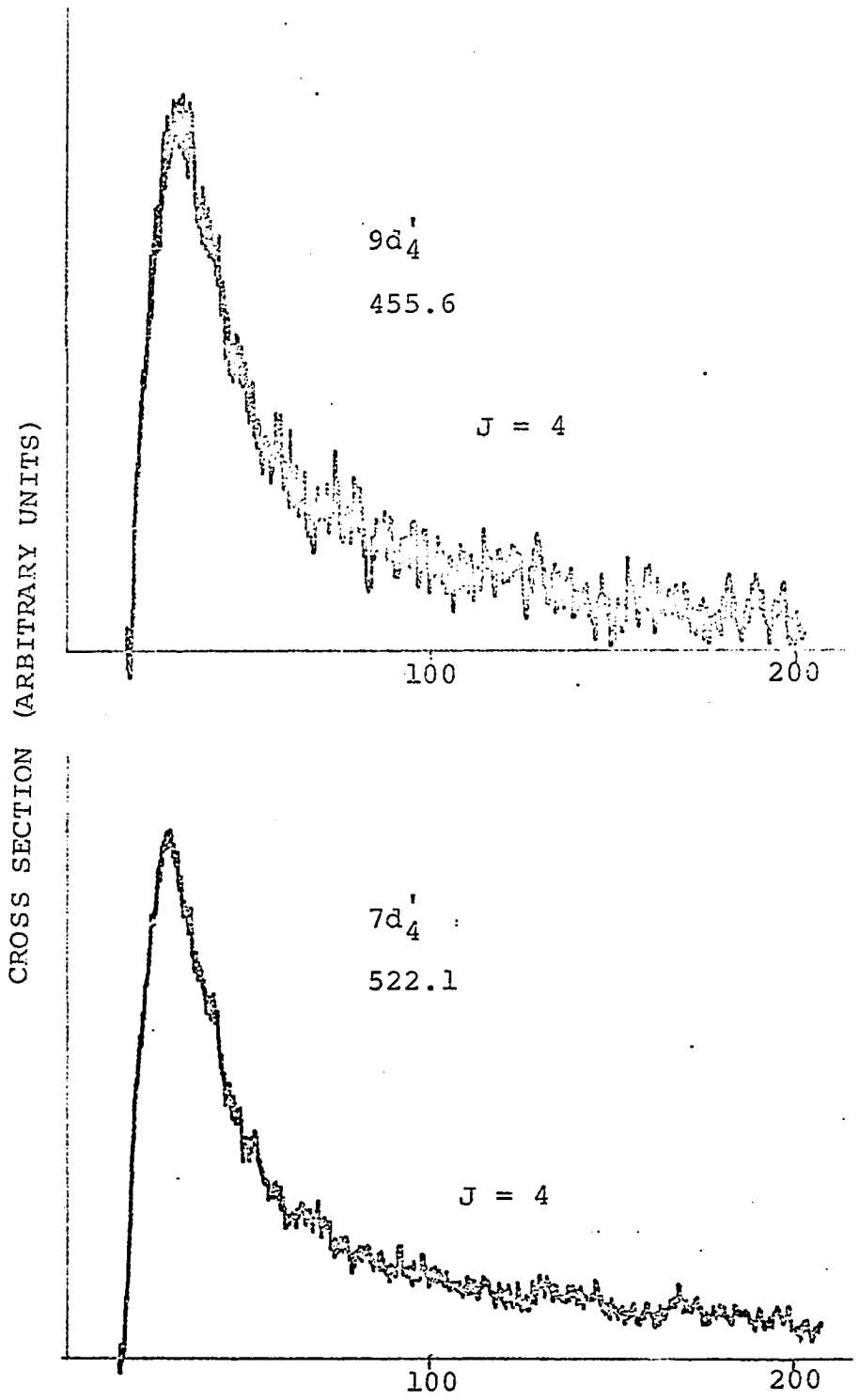

Figure 14. Excitation functions for $9d_4'$ and $7d_4'$.

CHAPTER VI

SUMMARY

The qualitative feature of the excitation functions of the levels of the $3p^5ns$, $3p^5np$, and $3p^5nd$ configurations reported in this paper can be explained by generalizing the results observed for helium along with a general theoretical consideration developed in Ref. 11. Within a given configuration $3p^5n\ell$, the states with odd values of $J+\ell$ are found to have larger cross sections than the even-$(J+\ell)$ states at incident energies well above the excitation threshold. Furthermore it was observed that in general $Q(J=0) > Q(J=2)$, $Q(J=1) > Q(J=3)$ for the np states, and $Q(J=2) > Q(J=0,4)$ for nd. These observations are in good agreement with the predictions of theory. Calculations of the excitation cross sections have been made, by Fajen[15], of the odd-$(J+\ell)$ states by means of the Born approximation based on Hartree-Fock-Slater type wave functions (with a semiempirical treatment of the fine-structure vector coupling). The discrepancy between the calculated and experimental values ranges from 24 per cent ($2p_1$) to a factor of 8 ($2p_8$) for the 2p states, and from 20 per cent to a factor of 8 for the 3p states, and from 20 per cent to a factor of 3 for 4d. It is felt that the disagreement between theory and experiment is to a large

measure due to the inaccuracy of the wave functions, particularly the semiempirical method for determining the coefficients of expansion of the wave functions in terms of the LS-eigenfunctions.

To convert the measured optical excitation cross sections into the apparent cross sections, it is customary to multiply the former by the appropriate branching ratios obtained from the theoretical transition probabilities. For atoms with complex structure like argon, the use of the theoretical transition probabilities may result in a rather large uncertainty in some of the apparent excitation cross sections. In this paper we have eliminated this source of inaccuracy by determining the branching ratios experimentally from measurements of relative intensities in an argon discharge tube. Since in our laboratory we are not equipped for vacuum ultraviolet work and the detection sensitivity at wavelengths above 1000 nm decreases markedly, we were not able to measure the relative intensities for all the lines necessary to obtain the branching ratios of a number of states, notably the 3p and 3s groups. To use the optical method effectively for determining excitation cross sections it should be very desirable to extend the frequency range of sensitive detection to both vacuum ultraviolet and the entire infrared region.